













Cite this: *Phys. Chem. Chem. Phys.*,  
2025, 27, 15080

# The structure of the NiO<sub>2</sub>N<sub>2</sub> coordination center in the [Ni(Salen)] complex and its polymer: a comparative study by X-ray absorption spectroscopy and quantum-chemical calculations†

Petr M. Korusenko, \*<sup>ab</sup> Olga V. Petrova, <sup>ac</sup> Anatoliy A. Vereshchagin, <sup>d</sup>  
Oleg V. Levin, <sup>d</sup> Evgeny V. Khramov, <sup>e</sup> Ratibor G. Chumakov, <sup>e</sup>  
Mikhail A. Soldatov, <sup>f</sup> Konstantin P. Katin, <sup>g</sup> Alexander S. Konev <sup>d</sup> and  
Alexander S. Vinogradov <sup>a</sup>

The atomic-electronic structure of the [NiO<sub>2</sub>N<sub>2</sub>] coordination center in the [Ni(Salen)] complex and its polymer was studied using X-ray absorption spectroscopy (EXAFS and NEXAFS) techniques, supplemented by quantum chemical calculations. Density functional theory (DFT) calculations were performed to construct the initial models of the [Ni(Salen)] complex and identify structural fragments of the poly-[Ni(Salen)] polymer that determine its properties in both reduced (Red) and oxidized (Ox) states. Based on the analysis of the Ni 1s EXAFS spectra, a d–d dimer model was found to best describe the structure and properties of the complex in the condensed state and can also be used as a simplified model for the polymer. It has been established that when moving from the complex to the poly-[Ni(Salen)]-Red, the square-planar structure of the [NiO<sub>2</sub>N<sub>2</sub>] coordination center remains practically unchanged. However, during the oxidation of the monomers, the coordination center becomes distorted, which is most likely caused by the phenolate–quinone transformation of the ligand. The absorption bands in the Ni 1s NEXAFS spectra of the complex and its polymer are attributed to Ni 1s electron transitions to vacant molecular orbitals (MOs) of the NiO<sub>2</sub>N<sub>2</sub> quasi-molecule. In order to determine the final structural fragments responsible for the properties of the complex and polymer in both charge states, we compared the experimental Ni 1s spectra with the model spectra calculated using the self-consistent Green's function method. It was found that the d–d stacked dimer is the basic structural unit that best describes the complex in its condensed state. In the case of the polymers, these structures are tetramers formed by the cross-linking of d–d dimers with total charges of 0 (reduced state) and +3 (with the BF<sub>4</sub><sup>−</sup> counterion, oxidized state). A joint analysis of the Ni 1s and 2p<sub>3/2</sub> NEXAFS spectra revealed that the local electronic structure of the coordination center in the complex and poly-[Ni(Salen)]-Red is characterized by a similar vacant antibonding MO. In contrast, for poly-[Ni(Salen)]-Ox, a new low-energy band appears in the Ni 2p<sub>3/2</sub> spectrum. This is due to Ni 2p<sub>3/2</sub> electron transitions to σ<sub>b1g</sub> MOs localized on Ni atoms with a reduced effective charge due to interactions with BF<sub>4</sub><sup>−</sup> counterions.

Received 14th April 2025,  
Accepted 23rd June 2025

DOI: 10.1039/d5cp01410g

rs.c.li/pccp

<sup>a</sup> V.A. Fock Institute of Physics, St. Petersburg State University, 7/9 Universitetskaya nab., 199034 Saint Petersburg, Russia. E-mail: korusenko\_petr@mail.ru

<sup>b</sup> Department of Physics, Omsk State Technical University, 11 Mira prosp., 644050 Omsk, Russia

<sup>c</sup> Institute of Physics and Mathematics, Komi Science Centre, Ural Branch of the Russian Academy of Sciences, 167982 Syktyvkar, Russia

<sup>d</sup> Institute of Chemistry, St. Petersburg State University, 7/9 Universitetskaya nab., 199034 Saint Petersburg, Russia

<sup>e</sup> Kurchatov Synchrotron Radiation Source, National Research Center Kurchatov Institute, Moscow 123182, Russia

<sup>f</sup> The Smart Materials Research Institute, Southern Federal University, Sladkova 178/24, 344090 Rostov-on-Don, Russia

<sup>g</sup> Department of Condensed Matter Physics, National Research Nuclear University "MEPhI", Kashirskoe Sh. 31, 115409 Moscow, Russia

† Electronic supplementary information (ESI) available: Additional data include raw Ni 1s XAFS spectra, EXAFS data and calculated data. See DOI: <https://doi.org/10.1039/d5cp01410g>

# 1. Introduction

Electrically conductive polymers obtained by electrochemical polymerization of planar complexes of 3d transition metals ( $M = V, Cr, Mn, Fe, Co, Ni, Cu$ ) with tetradentate  $N_2O_2$  Schiff base ligands (the so-called salen complexes ( $[M(\text{Salen})]$ )) are promising materials in numerous applications ranging from the development of antibacterial drugs to the creation of industrial catalysts and electrodes for electrochemical energy storage devices.<sup>1–5</sup> The main advantages of these polymers are due to the ability of the coordination  $[MO_2N_2]$  centers of the  $[M(\text{Salen})]$  monomers to participate in redox reactions. In this case, the conductivity between these centers, *i.e.* charge transfer, is ensured by the  $\pi$ -conjugated electronic system of the monomers.<sup>5</sup> For this reason, poly- $[M(\text{Salen})]$  films are actively studied using various experimental techniques, such as cyclic voltammetry and chronoamperometry, *in situ* UV-visible and infrared spectroscopy, electron paramagnetic resonance and ellipsometry.<sup>1–17</sup> However, the methods used provide far from a complete understanding and description of the processes of formation of these systems and, as a consequence, their structure. As a result, there is no consensus on the mechanism of polymerization of monomeric  $[M(\text{Salen})]$  molecules.

Currently, there are three different models of polymer formation. The first model assumes chemical linkage between the phenyl groups of the ligands of neighboring molecules and the formation of a chain-like structure.<sup>10</sup> In this case, the polymer is obtained as a result of the formation of  $\sigma$ -type covalent chemical C–C bonds between carbon atoms in the *para* positions of phenyl fragments (Fig. 1a). The second model of the polymerization mechanism is based on processes

associated with the metal atom.<sup>18</sup> In this case, the complexing cation  $M(II)$  is first additionally oxidized due to the  $M(II) \rightarrow M(III) + e^-$  reaction, after which it can form a vertical stack of monomers. This stack-like structure is stabilized by the donor–acceptor bonding between the phenolic moiety of the ligand and the metal atom (denoted as  $\pi$ -d, see b1 in Fig. 1b) or between the metal atoms (denoted as d–d, see b2 in Fig. 1b) of neighboring monomer molecules. There is also a third, hybrid model,<sup>18</sup> which combines both concepts: a  $\pi$ -d (c1) or d–d (c2) stack-like structure is initially formed, followed by cross-linking of individual stacks through the formation of covalent C–C bonds (Fig. 1c). The result is a strong mesh structure.

In view of the above, it should be noted that for the use of electrically conductive redox poly- $[M(\text{Salen})]$  polymers in modern technologies, detailed knowledge of the processes of electropolymerization of their monomer fragments is required. To do this, it is important to obtain information about the chemical (charge) state of the metal and ligand atoms, as well as to quantitatively characterize the parameters of the local atomic structure, in particular, the interatomic distances  $R(M-N)$  and  $R(M-O)$  of coordination  $[MO_2N_2]$  centers in monomers and their changes in poly- $[M(\text{Salen})]$  polymers in different (oxidized or reduced) states. This information can be obtained using modern X-ray spectroscopy methods: near edge X-ray absorption fine structure (NEXAFS) and extended X-ray absorption fine structure (EXAFS) spectroscopy.<sup>19–25</sup>

NEXAFS spectroscopy is used to obtain information about low-lying unoccupied electronic states in a polyatomic system and is based on the analysis of absorption bands in the immediate vicinity of the X-ray absorption edge – about 10 eV below and 30 eV above the absorption edge.<sup>19–22</sup> It is conventional to describe these spectra using multiple (resonant) scattering of low-energy ( $< 30$  eV) photoelectrons ejected from the core of an absorbing atom by the nearest neighbor atoms.<sup>19–22</sup> At certain core photoelectron energies, a quasi-molecule formed by absorbing and neighborhood atoms can temporarily trap the photoelectron, resulting in the formation of metastable excited states (shape resonances) of this quasi-molecule.<sup>20</sup> These resonances, depending on their lifetime, are observed in the absorption spectrum as narrow intense lines or broad, less intensive bands. The localization of the resonances within the quasi-molecule allows us to consider them also as a result of dipole-allowed transitions of core electrons to the unoccupied molecular orbitals (MOs) of this polyatomic system.<sup>20</sup>

In turn, the structure of EXAFS spectra of the absorbing atom is determined by the processes of single scattering of high-energy ( $> 50$  eV) photoelectrons by atoms of its nearest surroundings. These spectra represent a set of broad low-intensity absorption oscillations in the photon energy range from 50 to  $\sim 1500$  eV (with a photoelectron wave vector  $k$  from  $\sim 3.6$  to  $\sim 20 \text{ \AA}^{-1}$ ) above the absorption edge and make it possible to determine distances and coordination numbers around a specific absorbing atom with fairly high accuracy, thus providing probing of the local atomic structure of a polyatomic system in the vicinity of the absorbing atom.<sup>23–25</sup>

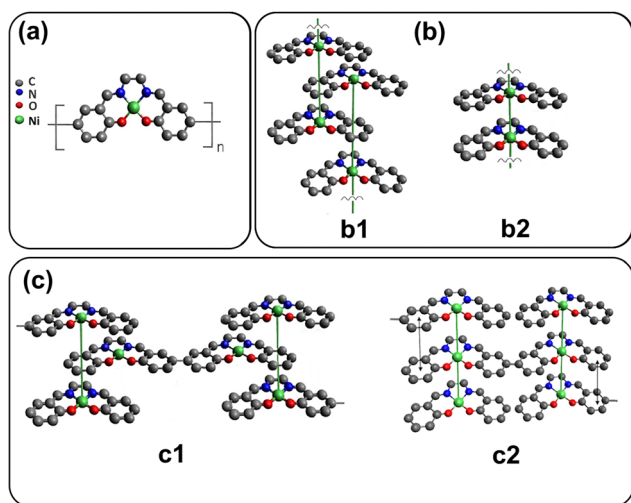


Fig. 1 Possible models of polymerization of the  $[Ni(\text{Salen})]$  complex: (a) model 1 – formation of chain-like structures through the C–C chemical linking between phenyl rings of neighboring monomers; (b) model 2 – formation of a stack-like structure due to the donor–acceptor interaction between the  $\pi$ -type AOs of the carbon and the metal atoms (b1 –  $\pi$ -d stacked structure) or  $\pi$ -type AOs of metal atoms (b2 – d–d stacked structure) of neighboring monomers; (c) model 3 – a hybrid variant combining both models (cross-linking of individual  $\pi$ -d (c1) or d–d (c2) stacks).

However, the application of NEXAFS and EXAFS techniques for the characterization of  $[\text{M}(\text{Salen})]$  monomers and their polymers is still limited to a few works,<sup>24,26–35</sup> in which X-ray absorption spectra of metal atoms were used mainly to check the purity and stoichiometry of the sample (Ni 1s NEXAFS,<sup>26,27</sup> Co 1s NEXAFS,<sup>33,34</sup> Cu 1s NEXAFS<sup>32,35</sup>) or to characterize the atomic coordination of the metal atom in the monomer<sup>32–34</sup> and polymer (Ni 1s, Ba 1s EXAFS,<sup>27,29</sup> Pd 1s EXAFS<sup>30</sup>).

In our previous works,<sup>36–38</sup> studies of the electronic structure of the  $[\text{Ni}(\text{Salen})]$  complex and salen ligand  $\text{H}_2(\text{Salen})$  were carried out using X-ray photoelectron (XPS) and photoemission spectroscopy (PES), including the resonance one (ResPES), NEXAFS spectroscopy with soft X-ray radiation, in the range of which are the 1s absorption edges of the ligand atoms (C, N, O) and 2p edges of the nickel atom. Analysis of these experimental spectra, supplemented by density functional theory (DFT) calculation data, allowed us to obtain new interesting information about (i) the directions of electron transfer between the complexing nickel atom and the ligand atoms, (ii) the atomic-orbital composition of MOs that determine the valence band of the  $[\text{Ni}(\text{Salen})]$  complex, (iii) the important role of the delocalized conjugated  $\pi$ -system of C 2p electronic states of the salen ligand in the processes of electronic redistribution, (iv) the presence among the unoccupied electronic states of a complex of empty  $\pi^*$ -MOs, reflecting the  $\pi$ -conjugation of oxygen (nitrogen) atoms with carbon atoms of phenol rings, *etc.* It should be emphasized that the performed measurements of the spectra of carbon, nitrogen and oxygen atoms were mainly focused on obtaining information about the properties of salen ligands, while new knowledge about the complexing nickel cation and the  $[\text{NiO}_2\text{N}_2]$  coordination center in general was very limited.

The main goal of this work is to obtain new information on the atomic-electronic structure of the  $[\text{Ni}(\text{Salen})]$  complex in the condensed state and its polymer based on a comparative analysis of the parameters of the  $[\text{NiO}_2\text{N}_2]$  coordination center established as a result of a detailed examination of the Ni 1s EXAFS and the Ni 1s(2p) NEXAFS spectra of these materials. For this purpose, the following studies were performed: (i) measurements of Ni 1s EXAFS and Ni 1s(2p) NEXAFS spectra of  $[\text{Ni}(\text{Salen})]$  and poly- $[\text{Ni}(\text{Salen})]$  in different charge states; (ii) obtaining data about the geometry and  $R(\text{Ni}-\text{N})$ ,  $R(\text{Ni}-\text{O})$  interatomic distances for the  $[\text{NiO}_2\text{N}_2]$  coordination center in the complex and their changes upon transition to the poly- $[\text{Ni}(\text{Salen})]$  polymer in the oxidized and reduced states based on Ni 1s EXAFS spectra; (iii) an identification of structural units (fragments) responsible for the basic properties of the complex in the condensed state and its polymer using  $R(\text{Ni}-\text{Ni})$  data for neighboring monomers from EXAFS spectra and the results of quantum chemical calculations; (iv) characterization of the chemical (charge) state of the Ni atom and the local electronic structure near it for the compared systems based on a comparative analysis of Ni 1s and 2p NEXAFS spectra; (v) a final examination of the derived structural fragments by a detailed comparison of the Ni 1s NEXAFS spectra which were measured and simulated on the basis of quantum-chemical calculations for structural units of the complex in the condensed state and its polymer in various charged (oxidized and reduced) states.

## 2. Materials and methods

### 2.1. Sample preparation

The molecular complex  $[\text{Ni}(\text{Salen})]$  was synthesized in a powder form using the standard procedure<sup>39,40</sup> by adding nickel acetate  $\text{Ni}(\text{Ac})_2$  to the ethanol solution of  $\text{H}_2(\text{Salen})$ . The resulting powder was purified by recrystallization from a solution in ethanol followed by drying under vacuum at 80 °C. Polymer films of poly- $[\text{Ni}(\text{Salen})]$  were prepared onto a flat Pt electrode by electropolymerization from 0.001 M monomer solution in the 0.1 M  $\text{LiBF}_4/\text{CH}_3\text{CN}$  electrolyte in cyclic voltammetry (CV) mode using an Autolab PGSTAT30 potentiostat (Fig. 2). When synthesizing polymer films, a three-electrode cell with a reference electrode filled with a 0.1 M  $\text{Et}_4\text{NBF}_4/\text{CH}_3\text{CN}$  solution containing 0.001 mol  $\text{L}^{-1}$   $\text{AgNO}_3$  (MF-2062, Bioanalytical systems) was used. The potential of such a reference electrode relative to  $\text{Ag}|\text{AgCl}$  filled with a saturated NaCl solution was +0.25 V, wherein stainless-steel wire mesh was utilized as a counter electrode. To prepare polymers in different charge states, after several polymerization cycles, when a given potential was reached, the synthesis was stopped, namely: the potential value of  $-0.2$  V corresponded to the reduced state (Red) and +1.0 V to the fully oxidized state (Ox) (Fig. 2). Then the prepared films were thoroughly washed in  $\text{CH}_3\text{CN}$  and dried. The thickness of the polymer films was about  $\sim 30$  and  $\sim 450$  nm, which corresponded to 2 and 15 polymerization cycles at a potential scan rate of  $50 \text{ mV s}^{-1}$ , respectively. All samples were prepared in an argon-purged glovebox and then sealed in Eppendorf tubes to reduce environmental interaction and subsequent degradation.

### 2.2. Methods

**2.2.1. Ni 1s NEXAFS and EXAFS spectroscopy.** All studies were performed at the “KISI-Kurchatov” synchrotron radiation (SR) source (Moscow);<sup>41</sup> Ni 1s NEXAFS and EXAFS experiments were carried out using the “Structural Materials Science” end-station.

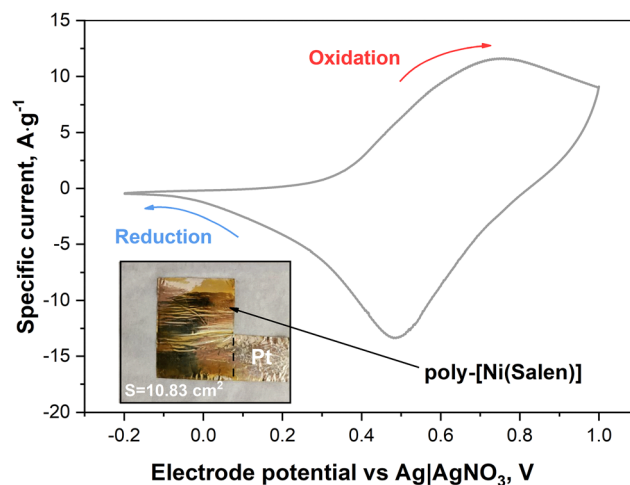


Fig. 2 The cyclic voltammogram of the anodic polymerization of  $[\text{Ni}(\text{Salen})]$  at a Pt-electrode, between  $-0.2$  and  $+1.0$  V at the scan rate of  $50 \text{ mV s}^{-1}$  (after 15 deposition cycles). The inset shows a photograph of a Pt-electrode after 15 cycles of  $[\text{Ni}(\text{Salen})]$  polymerization.

For Ni 1s NEXAFS and EXAFS measurements, the [Ni(Salen)] powder was pre-ground for 10 min in an agate mortar. Then, a tablet of approximately 0.5 mm thickness was prepared by pressing the prepared monomer powder (~20 mg) together with finely dispersed hexagonal boron nitride (h-BN) (~100 mg), which acted as a binder. An important advantage of h-BN is also that it is chemically inert and it weakly absorbs X-rays in the Ni 1s absorption edge region. Polymer films were attached to sample holders without additional processing using conductive double-sided tape. Monochromatization of the “white SR beam” was performed using a Si(111) single crystal monochromator of the “channel-cut” type with a fixed output. Ni 1s absorption spectra were recorded in the photon energy range from 8100 to 9130 eV (Fig. S1, ESI†), which was -250 eV before and 800 eV after the absorption edge, respectively. The EXAFS signal extraction range for the complex and its polymer was 2 to 13 and 2 to 10 Å<sup>-1</sup> in *k*-space, respectively. The energy resolution of the monochromator in the region of the Ni 1s absorption edge (~8333 eV) was about 1 eV. The scanning step in the NEXAFS region was  $\delta E \sim 0.35$  eV. In the EXAFS region the step was variable, in order to correspond to  $\delta k \sim 0.05$  Å<sup>-1</sup>. An internal nickel foil standard (Ni<sup>0</sup>) was used to calibrate the energy on each scan, allowing continuous monitoring of the energy scale. The process itself consisted of determining the energy shift ( $\Delta E$ ) of the main maximum of the first derivative of the nickel foil spectrum and adjusting it to the energy position of the Ni 1s absorption edge of metallic nickel at a photon energy of  $E_0 = 8333$  eV.<sup>42</sup> Then the Ni 1s absorption spectra of the samples were corrected by the  $\Delta E$  value.

All measurements for the monomer were carried out in the transmission mode. In this case, the intensity ( $I_0$ ) of the X-ray beam incident on the sample was measured using a free-air ionization chamber, while an argon-filled chamber was used to measure the intensity ( $I_1$ ) of the X-ray beam passing through the sample. The spectrum of the Ni foil was measured simultaneously with the spectrum of the sample using an X-ray beam passing through the first two ionization chambers and the sample under study as well as an additional argon-filled ionization chamber. Keithley digital picoammeters were used to take signal readings in the ionization chambers. As a result, for the sample the absorption coefficient  $\mu_1(E)$  is calculated using the formula  $\mu_1(E) = \ln(I_0/I_1)$ , while for the Ni<sup>0</sup> standard  $\mu_2(E) = \ln(I_1/I_2)$ . Here  $I_2$  is the intensity of the X-ray beam passed through the standard, which is measured using the total absorption detector. Normalization of transmission spectra was performed in the IFEFFIT ver. 1.2.11 software package by subtracting the pre-edge and post-edge background (selected by a polynomial from the pre-edge region analysis, which then approximated the background) followed by dividing each spectrum by the height of its absorption jump.

The Ni 1s spectra of polymers were recorded in fluorescence measurement mode using a KETEK X1272 silicon drift detector (SDD) with an energy window of 100 eV, which was connected to an Amptek DP5 high-performance pulse analyzer. When registering the fluorescence signal, polymer films were placed at an angle of 45° to the X-ray beam and only Ni K $\alpha$  photons were recorded. For polymer films, the absorption coefficient

$\mu(E)$  was calculated using the formula  $\mu(E) = I_f/I_0$ , where  $I_f$  is the fluorescence signal from the sample and  $I_0$  is the intensity of the X-ray beam incident on the sample. At the same time the signal from the standard (Ni<sup>0</sup> foil) was recorded in transmission mode on the residual beam after the second ionization chamber. It is important to note that the strong self-absorption effect in the fluorescence Ni 1s absorption spectra of polymers was not observed, which is due to the low concentration of the element (Ni) under study in the samples (2–5 at%), as well as the small film thickness of about 450 nm. In confirmation of the above, it was shown in the work<sup>43</sup> that for iron oxide films less than 1  $\mu$ m thick, the intensity of Fe K $\alpha$  fluorescence has an almost linear dependence on the absorption coefficient, which indicates that there is no need to correct for self-absorption. Therefore, additional spectral correction for spectra for polymers was not required. Thus, this fact allows us to conduct a direct comparative analysis of the absorption spectra for the complex in the transmission mode and for the polymer in the fluorescence mode.

The absorption spectrum of the complex was recorded in transmission mode in 20 minutes, and the spectrum of the polymer in X-ray fluorescence mode was accumulated in 30 minutes. To increase the signal-to-noise ratio, measurements for each sample were repeated at least 2 times in transmission mode and 4 times in fluorescence mode, followed by averaging of the resulting spectra. All EXAFS and NEXAFS measurements were performed under atmospheric conditions.

**2.2.2. Ni 2p<sub>1/2,3/2</sub> NEXAFS spectroscopy.** The Ni 2p<sub>1/2,3/2</sub> NEXAFS spectra of [Ni(Salen)] and poly-[Ni(Salen)] were recorded using a “NanoPES” end-station at the “KISI-Kurchatov” SR source.<sup>44</sup> These measurements for the [Ni(Salen)] complex were carried out using thin layers (~20–50 nm) on a Pt plate prepared by thermal evaporation of a dehydrated powder from a quartz crucible, as described in ref. 36 and 37. In the case of poly-[Ni(Salen)], the as-prepared 30 nm thick polymer layers on a Pt substrate were preheated at approximately 190 °C for 30 min before being used as samples for measurement. Photon energy resolution in the vicinity of Ni 2p<sub>3/2</sub> (~850 eV) absorption edge was 300 meV. All NEXAFS spectra were normalized to the incident photon flux, which was monitored by recording photocurrent from a clean gold mesh. Photon energy was calibrated by measuring the Pt 4f<sub>7/2</sub> PE line excited by radiation in the first and second diffraction orders and taking their difference. The measurements were carried out at room temperature and a residual pressure of about  $2 \times 10^{-10}$  mbar. No noticeable effects of charging or deterioration of the [Ni(Salen)] samples irradiated by intense synchrotron beam were observed. The NEXAFS spectra from the evaporated [Ni(Salen)] sample and polymer samples were registered several times from different points on the sample, and their structure usually showed good reproducibility.

### 2.3. Theoretical models, DFT calculations, analysis of EXAFS and NEXAFS spectra

To obtain the desired structural information from the Ni 1s EXAFS and NEXAFS spectra of the complex, its polymer, monomer and stack-like dimer structural models were constructed and analyzed for the [Ni(Salen)] complex using DFT calculations

(Fig. 3a and b). The initial values of the structural parameters for constructing these fragments were taken from ref. 45. In the case of the polymer, the tetramer and stack-like d-d dimer models were used. The tetramer model is two horizontally arranged d-d-dimers, in which two monomers of one layer are linked by a C-C bond between the phenyl rings (Fig. 3c). In this case, one additional phenyl ring was added to the two unlinked monomers located in the upper layer of this structure at each edge. This approach allows one to take into account the subsequent polymerization process of the structure by forming C-C bonds with the next similar fragments on the left and right. In other words, the proposed tetramer model has a periodic structure and can be considered as a single fragment of the poly-[Ni(Salen)] polymer.

All DFT calculations were performed using the GAMESS-US software.<sup>46</sup> The geometries of the monomer, dimer, and tetramer were optimized using the B3LYP functional.<sup>47,48</sup> When optimizing the geometry of the monomer and dimer structures, the total charge was set to  $q = 0$ . For the tetramer, the optimization was performed at a total charge of  $q = 0$ , as well as +1, +2, +3, +3 (with the  $\text{BF}_4^-$  counterion) and +4 to simulate the reduced and charged (oxidized) states of the polymer. Electronic multibasis was constructed from 311+G\*\* basis functions of organic ligands and lanl2tz+ basic functions of Ni atoms.<sup>49</sup> The geometries of all structures were optimized without any restrictions on symmetry, and the residual forces did not exceed  $10^{-4}$  eV  $\text{\AA}^{-1}$ .

Ni 1s EXAFS data were analyzed using the Athena and Artemis program versions 0.8057.0.0 and 0.8012.0.0 respectively, included in IFEFFIT version 1.2.11,<sup>50</sup> by cutting the oscillating part of the normalized X-ray spectrum (EXAFS oscillations) with further data conversion to  $k$ -space (signal  $\chi(k)$  data) and the Fourier transform to  $R$ -space (signal  $\chi(R)$  data). The EXAFS  $\chi(k)$  function can be written in general form as the sum of contributions from all scattering paths of a photoelectron that passes from the absorbing atom (in our case it is the Ni atom) and then scatters from neighboring atoms (nitrogen, oxygen and carbon) and eventually returns to the absorbing atom:<sup>23,25</sup>

$$\chi(k) = \sum_i \frac{N_i \cdot S_0^2 \cdot f_i^{\text{eff}}(k) \cdot e^{-2k^2 \cdot \sigma_i^2}}{k \cdot R_i^2} \cdot \sin[2k \cdot R_i + \delta_i(k)] \cdot \exp\left(\frac{-2R_i}{\lambda(k)}\right) \quad (1)$$

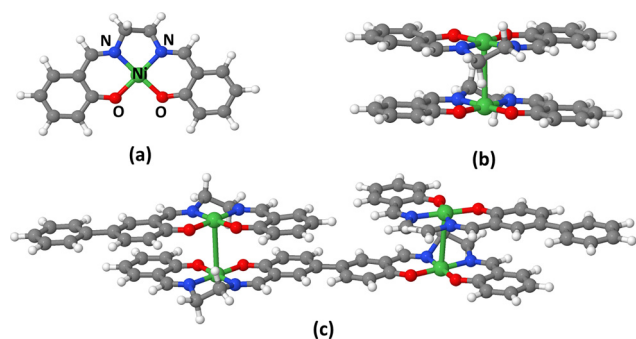


Fig. 3 Unoptimized structures of the monomer (a), d-d dimer (b) and tetramer (c). Carbon and hydrogen atoms are represented by gray and white balls, respectively.

where  $f_i^{\text{eff}}(k)$ ,  $\delta_i(k)$ ,  $\lambda(k)$  and  $k$  are the effective scattering amplitude, phase shift, mean free path of the photoelectron and photoelectron wave vector, respectively. It follows from the formula (1) that the summation is carried out over all possible scattering paths of photoelectron  $i$ , characterized by the effective path length  $R_i$ . The factor  $N_i$  determines the number of such identical indistinguishable paths, and  $S_0^2$  takes into account the effects of multielectron excitation and excitation of the entire system of atoms, ignored by the original model of the single-particle approximation. In addition, this formula also takes into account the root-mean-square change in the length of the effective scattering path, which is determined by the Debye-Waller factor, denoted  $\sigma_i^2$ . To extract information about the coordination spheres from the EXAFS oscillations, the Fourier transform of the  $\chi(k)$  spectrum into  $R$ -space was performed. For this, the  $\chi(k)$  function was multiplied by a weight function of the  $k^2$  type so that the amplitude of the  $k^2 \cdot \chi(k)$  function was approximately constant over the entire  $k$  region in which the spectrum was recorded. The final stage of processing the EXAFS data is finding a set of structural parameters ( $R_i$ ,  $N_i$ ,  $S_0^2$  and  $\sigma_i^2$ ) for which the theoretically calculated spectrum best describes the experimental curve.

DFT-optimized monomer and d-d dimer models were used as input parameters for fitting the experimental EXAFS data for the complex. DFT-optimized tetramer structures with different total charges (from 0 to +4) and dimers were considered as potential models for the poly-[Ni(Salen)] polymer in different charge states.

Modeling of the Ni 1s NEXAFS spectra was used to qualitatively assess the suitability of the constructed DFT-optimized structures of the monomer, dimer and tetramer with  $q = 0, +3, +3$  (with the  $\text{BF}_4^-$  counterion) for describing the atomic and electronic structure of the complex and its polymer, respectively. The simulations have been performed for neutral molecules using self-consistent Green's function method as well as the finite difference method implemented within the FDMNES program package.<sup>21,51</sup> When optimizing the calculation parameters both for matching the electronic structure and for calculating the spectrum shape, the core vacancy was taken into account without screening, which made it possible to obtain better agreement between theory and experiment. The optimal cluster radius for the calculation was chosen to be 12  $\text{\AA}$ , taking into account the fact that all atoms within one [Ni(Salen)] molecule were expected to be within this range. Thus, for the monomer, dimer, and tetramer, theoretical Ni 1s spectra were obtained for each nickel atom in the model. In the case of the dimer and tetramer, the modeled spectra for each nickel atom were summed up, and the total spectrum was used further. The results of this simulation of Ni 1s spectra were then used for comparison with experimental spectra to identify the structural units of the complex in the condensed state and its polymers in the oxidized and reduced states. For this purpose, the energy alignment of the theoretical Ni 1s spectra to the experimental ones was done by adjusting the calculated Fermi level.

A detailed analysis of the fine structure of the Ni 1s and  $2p_{3/2}$  NEXAFS spectra of the complex and its polymer was performed

within the framework of a quasi-molecular approach, namely, absorption peaks were associated with the dipole-allowed transitions of Ni 1s and 2p<sub>3/2</sub> electrons into unoccupied MOs of the NiO<sub>2</sub>N<sub>2</sub> quasi-molecule, which is formed by the absorbing nickel atom and the atoms of its nearest surroundings.

### 3. Results and discussion

#### 3.1. Theoretical models

We begin the discussion of the results by examining the theoretical models for the complex and its polymer, which are presented in Fig. 4. According to the research data,<sup>45,52,53</sup> two models can be considered to describe the structure of the [Ni(Salen)] complex: a monomer and a d-d dimer (Fig. 4a and b). At the same time, due to the lack of appropriate crystallographic data for the poly-[Ni(Salen)] polymer, we had to construct six different models based on tetramers with different total charges ( $q$ ) when performing DFT optimization (Fig. 4c–e and Fig. S2, ESI<sup>†</sup>). In a previous study,<sup>54</sup> poly-[Ni(Salen)] was modeled as the periodic structure on tetramers without C–C bonding, with the polymer bearing the charge of  $q$  between 0 and +4 to describe different oxidation states (Fig. 4c). However, later studies<sup>40,55</sup> showed that the structure of poly-[Ni(Salen)] includes C–C bonding between ligands of different monomers. Therefore, the d–d model reported in ref. 54 should be improved to better represent the structure of this material. To simplify the computational task, we approximated the periodic structure of poly-[Ni(Salen)] polymer by

model compounds based on four monomeric [Ni(Salen)] units, two of which are linked by a C–C bond.

The oxidized conducting form of the poly-[Ni(Salen)] polymer contains mainly polarons of radical-cation nature with some contribution of bipolarons. In the d–d model,<sup>54</sup> the polarons were simulated by the high-spin state of tetramers with  $q = +2$  (removing 0.5 electrons from each monomer), while bipolarons were modelled by low-spin tetramers with a total charge of +4 (removing one electron from each monomer). Therefore, the oxidation degree of a four-monomer unit should be between +2 and +4. Besides, the oxidation of a polymer film is accompanied by its doping with counterions to compensate for the arising positive charge. For this reason, we augmented the model by the addition of a BF<sub>4</sub><sup>−</sup> counterion to a tetramer with  $q = +3$  and re-optimizing this structure with the same total charge to account for the intermediate oxidation state between fully polaronic and fully bipolaronic states (Fig. 4d and e). Also, tetramers with  $q$  changing from +1 to +4 were analyzed for comparison (see Fig. S2 and Table S1, ESI<sup>†</sup>). According to DFT calculations, the excessive positive charge in the tetramer with  $q = +3$  is localized on the ligands, while the spin-density is localized on the bi-phenyl semi-quinone-like ligand, consistent with the expected radical cation nature of the polaron.

Data on the interatomic distances  $R(\text{Ni–N})$  and  $R(\text{Ni–O})$  of the coordination center for the DFT-optimized structures of the monomer, dimer, and tetramer are summarized in Table 1. These data show that the calculated interatomic distances  $R(\text{Ni–N})$  and  $R(\text{Ni–O})$  for the monomer generally correlate with the theoretical data obtained by Prof. Girichev's group. For the

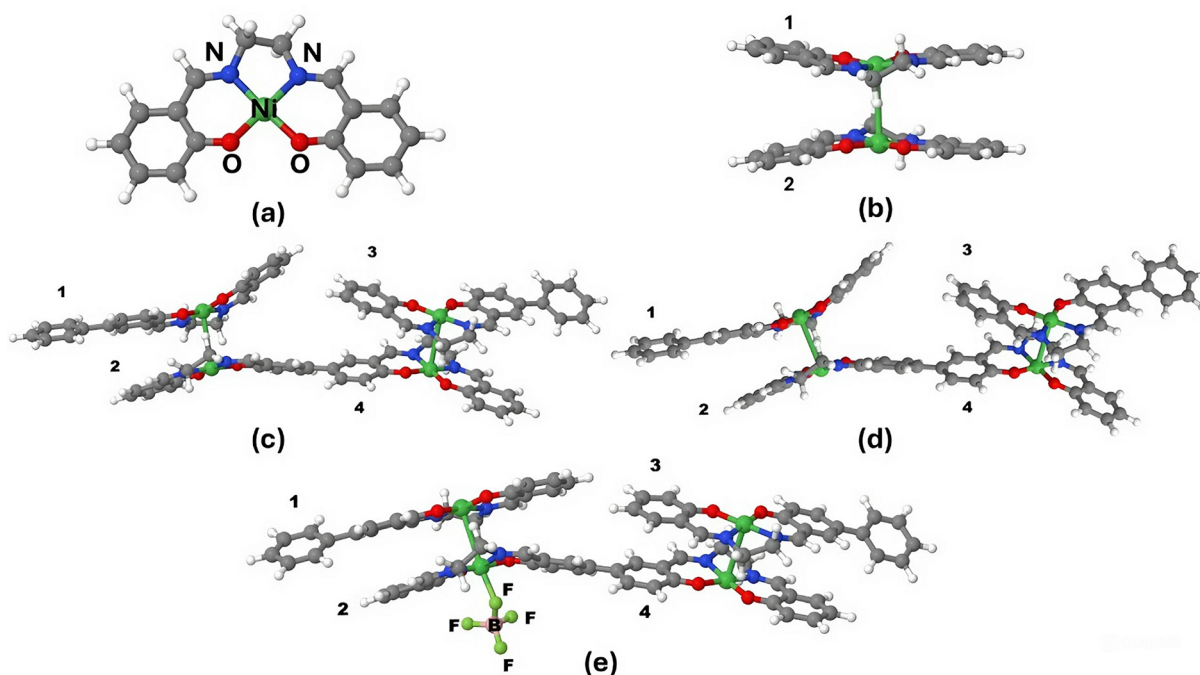


Fig. 4 DFT optimized structures of the monomer (a), d–d dimer (b) and tetramers: with total charge  $q = 0$  (c),  $q = +3$  (d) and  $q = +3$  (with the BF<sub>4</sub><sup>−</sup> counterion) (e). Carbon and hydrogen atoms are represented by gray and white balls, respectively. The numbers indicate the monomeric fragment number.

**Table 1** Interatomic distances  $R(\text{Ni-N})$  and  $R(\text{Ni-O})$  for the coordination center, as well as the  $R(\text{Ni-Ni})$  distance between monomers in model structures, obtained from DFT calculations

Structure	Interatomic distances, Å			Method	Ref.
	Ni-N	Ni-O	Ni-Ni		
Monomer	1.883	1.865	—	DFT (B3LYP/311+G**, lanl2tz+)	This work
Monomer	1.876	1.860	—	DFT (B3LYP/CEP-31G)	52 and 53
d-d Dimer	1.872	1.843	3.27	DFT (CAM-B3LYP-D3/6-31G(d))	9
d-d Dimer	1.885	1.870	3.66	DFT (B3LYP/311+G**, lanl2tz +)	This work
Tetramer, $q = 0$	1.862	1.821	3.33		This work
Tetramer, $q = +3$	1.857	1.812	3.26		This work
Tetramer, $q = +3$ (with $\text{BF}_4^-$ )	1.873	1.856	3.15		This work

dimer, these interatomic distances differ only slightly from those of the monomer. In the case of the tetramer models, there is a decrease in both the interatomic distances in the coordination centers compared to the dimer. At the same time, for the tetramer optimized at  $q = 0$ , the values of  $R(\text{Ni-N})$  and  $R(\text{Ni-O})$  decrease by 0.023 and 0.049 Å, respectively, and for the tetramer with  $q = +3$ , they decrease by 0.028 and 0.058 Å. The smallest changes were found for the  $\text{BF}_4^-$  doped tetramer with a charge of +3, by approximately  $-0.01$  Å for both interatomic distances. Thus, for the tetramer models with  $q = 0$  and +3, a distortion in the geometry of the square-planar structure of the coordination centers was observed compared to the dimer. However, this distortion was more pronounced for the tetramer optimized for  $q = +3$ . At the same time, although there are no significant changes in the square-planar structure based on the averaged values of  $R(\text{Ni-N})$  and  $R(\text{Ni-O})$  for the  $\text{BF}_4^-$  doped tetramer with  $q = +3$ , for this model, visible deviations in the interatomic distances between the nickel and oxygen (nitrogen) atoms are detected in fragments 2 and 4 (see Table S1, ESI†). In addition to the  $R(\text{Ni-N})$  and  $R(\text{Ni-O})$  data, it is also interesting to examine the change in the  $R(\text{Ni-Ni})$  distance between individual monomers when moving from the dimer model to the tetramer models. This parameter can be used to more accurately determine the appropriate model to describe the structural units (fragments) responsible for the main properties of the polymer, both in the (Red) and (Ox) charge states. It is clear that when moving from the dimer model to the tetramer models, the distance  $R(\text{Ni-Ni})$  decreases from 3.66 to 3.15 Å. This can be interpreted as the convergence of individual monomers in stacks. Here, the smallest value is observed in the case of a tetramer with  $q = +3$  with the  $\text{BF}_4^-$  counterion.

### 3.2. EXAFS

Let us now turn to the consideration of experimental Ni 1s EXAFS spectra for the complex and its polymer for which EXAFS functions ( $k^2\chi(k)$  oscillation signals) and their Fourier-transforms (FTs) are shown in Fig. 5a and b. The raw absorption spectra are presented in Fig. S1 (ESI)†. It can be seen that the EXAFS functions ( $k^2\chi(k)$ ) for all samples are well resolved in the  $k$ -space range of  $2\text{--}10 \text{ \AA}^{-1}$ , which has been taken as a range of Fourier transformation. The Fourier transforms of all spectra have four pronounced FT maxima, designated as P1, P2, P3 and P4 bands (Fig. 5b), and are located in the  $R$ -space range from 1 to 3.5 Å. In the case of the complex, the most intense P1 band corresponds to

the first coordination sphere around the absorbing Ni atom (Fig. 5c), which includes four atoms (two N atoms and two O atoms) and thus contains information on the interatomic distances  $R(\text{Ni-N})$ ,  $R(\text{Ni-O})$  and the geometry of the coordination center. The next two bands, P2 and P3, are associated with contributions from the second and third coordination spheres and are due to the photoelectron scattering by carbon atoms of the ethylenediamine and phenyl fragments (these atoms are designated as C2 and C3 and C4 and C5 in Fig. 5c). In addition, these bands can be affected by double photoelectron scattering from C and O/N atoms: Ni-C5-O, Ni-C3-N and Ni-C2-N. The probability of each double scattering path is relatively low, but due to the large degeneracy, *i.e.*, the large number of these similar paths, an influence on the intensity and shape of P2 and P3 bands can be significant. At the same time, the nature of the P4 band is likely related to photoelectron scattering by carbon atoms. However, it can only be determined more accurately by using different structural models.

Now let us consider the FT curves 2 and 3 (Fig. 5b) for EXAFS spectra of the polymer in the oxidized and reduced states. It is clearly seen that both FT curves contain the same number of bands in the  $R$  range of  $1\text{--}3.5 \text{ \AA}$  as the curve 1 for the monomer spectrum. A detailed examination of the shape of the P1 band reveals that for the polymer in its reduced state, the intensity and width at half maximum of this band are similar to those of P1 for the  $[\text{Ni}(\text{Salen})]$  complex (inset in Fig. 5b). At the same time, this band is less intense for the oxidized polymer, and its width,  $0.54 \text{ \AA}$ , is larger than that for the monomer ( $0.42 \text{ \AA}$ ). Additionally, the maximum of the P1 band is shifted towards lower  $R$  values. Based on these results, it is reasonable to assume that during the electrochemical oxidation (polymerization) of the  $[\text{Ni}(\text{Salen})]$  complex, there are changes in the interatomic distances  $R(\text{Ni-N})$  and  $R(\text{Ni-O})$  in the coordination center and the square-planar structure of the complex is violated. During the subsequent transition to a reduced polymer, it appears that the interatomic distances and geometry are partially restored.

The strategy for further EXAFS analysis is to obtain theoretical EXAFS spectra using model structures constructed based on DFT calculations and then compare them with experimental ones. This approach will allow us to determine changes in the interatomic distances  $R(\text{Ni-N})$  and  $R(\text{Ni-O})$  and the geometry of the coordination center in moving from the  $[\text{Ni}(\text{Salen})]$  complex to the poly- $[\text{Ni}(\text{Salen})]$  polymer and then compare the results

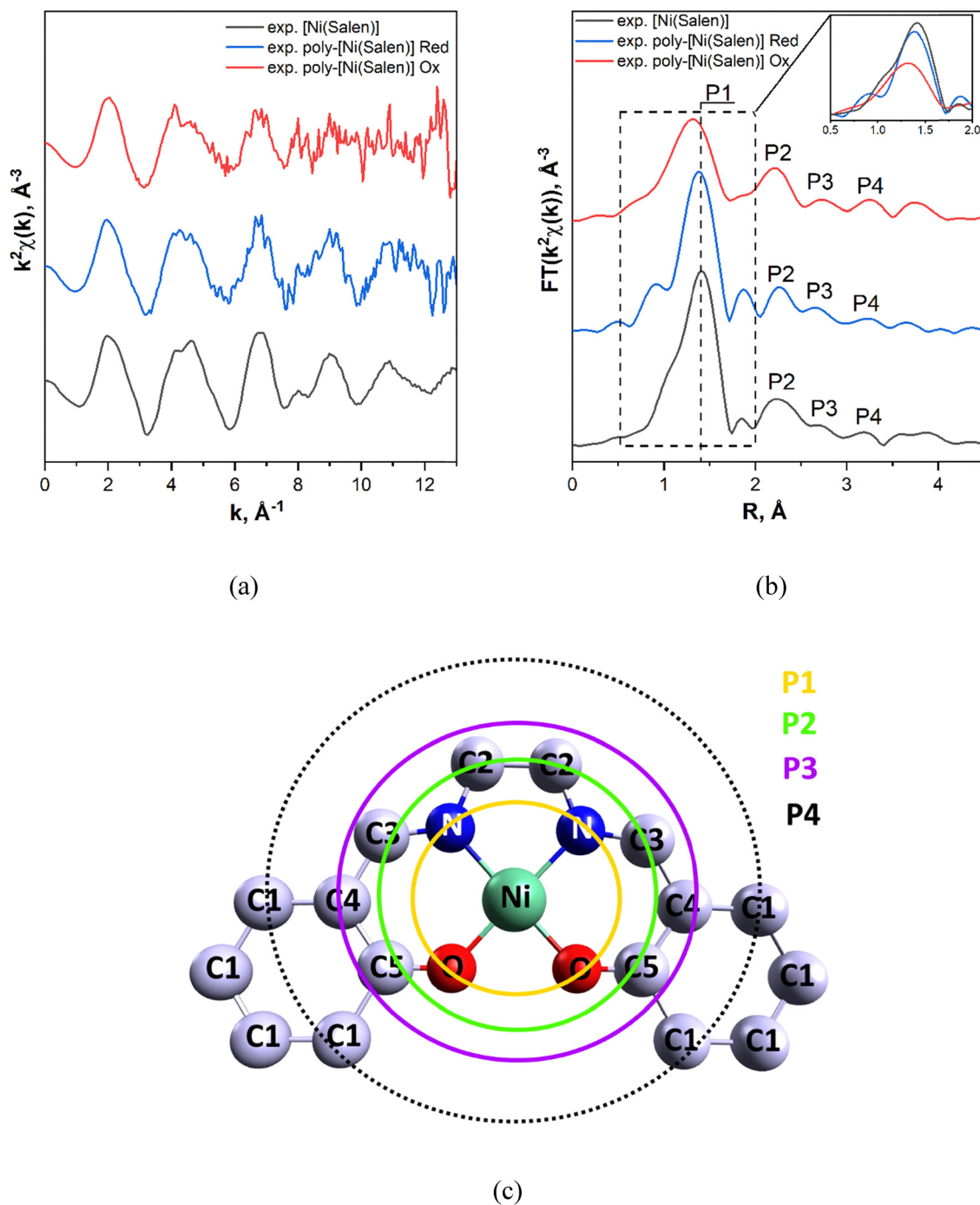


Fig. 5 Experimental  $k^2\chi(k)$  oscillation signals for Ni 1s EXAFS spectra (a) and their Fourier transforms (b) for the [Ni(Salen)] monomeric complex (black curve) and its polymer in Red (blue curve) and Ox (red curve) states. The diagram (c) shows four coordination spheres of the complex. The carbon atoms in the second, third and fourth spheres are divided into several numbered groups, C1, C2, C3, C4, and C5, with similar chemical states, as described in ref. 36.

with those obtained from DFT calculations. In addition, the data for the 2nd, 3rd and 4th coordination spheres will be analyzed to determine which atoms will make the greatest contribution to scattering by these shells for the complex and polymer and also how the distances between individual monomers in dimers for the oxidized and reduced polymers will change.

Before fitting FT curves for the experimental EXAFS spectra of our systems, we considered the approaches and analysis results obtained for the related complex based on [Ni(Salen)] and its polymer with the  $[\text{NiO}_2\text{N}_2]$  coordination center.<sup>27</sup> In this study, the monomer structure was used as a theoretical model to describe the FT curves of both the complex and its polymer. It is important to note that during the fitting process, the

authors used only one scattering path to describe the first coordination sphere. In other words, they combined the Ni–O and Ni–N scattering paths into one path. The interatomic distances  $R(\text{Ni–O/N})$  for the complex and the polymer were  $1.83 \pm 0.02$  and  $1.84 \pm 0.02$  Å, respectively. At the same time, these values were not different for the oxidized and reduced forms of the polymer. In the next second and third coordination spheres, closely spaced scattering paths were also combined into a single path. Therefore, it can be concluded that the authors' use of only the monomer model and a number of assumptions during fitting does not allow them to fully extract information about the geometry of the  $[\text{NiO}_2\text{N}_2]$  coordination center and its changes in going from the complex to polymer in oxidized and reduced forms.

Considering the above, we examined the results of the FT curve fitting for the experimental Ni 1s EXAFS spectrum of the complex, using theoretical data obtained for both the monomer and dimer structures (Fig. 6a). The fitting was performed within a range of interatomic distances  $R = 1.0\text{--}3.5$  Å from the Ni atom and included four coordination spheres for both the monomer and the d–d dimer. For these structures, the band (scattering path) P1 is the same. The first coordination sphere (P1) consists of four atoms of the coordination center (two N atoms and two O atoms). The second sphere (P2) is composed of four C atoms from the benzene rings (C3, C5) and two C atoms (C2) from the imine fragment  $\text{–C=N–}$ . In addition, in the case of the dimer structure, the double scattering path Ni–C5–O/Ni–C3–N, with a degeneracy factor of 12, is also taken into account. The third coordination sphere (P3) contains two C atoms from the benzene rings (C4), which are located at a distance  $R$  of

$\sim 3.0$  Å from the nickel atom (Fig. 5c and 6a). Also, for the monomer structure, a double scattering path is also taken into account, similar to that in the dimer structure, which contributes to the P2 band. The fourth coordination sphere (P4), in the case of the monomer model, is formed by four of the eight C1 atoms, which are closer to the Ni atom. In the case of the dimer structure, we assume that the P4 band includes contributions from the photoelectron scattering by Ni atoms of neighboring monomers (with an Ni–Ni interatomic distance) as well as from the double scattering path by the opposite atoms of the coordination center (Ni–N–O/Ni–O–N), with a degeneracy coefficient of 4. Thus, when constructing the theoretical model of the monomer, we used five photoelectron scattering paths, of which four were single and one double scattering path. In the case of the dimer, seven photoelectron scattering paths were used, with five single and two double scattering paths. For both models, two single scattering paths (Ni–O and Ni–N), which are close to each other in distance, were assigned to the same coordination sphere.

The results of the approximation for the first and fourth coordination spheres, including the parameters of the local structure of the  $[\text{Ni}(\text{Salen})]$  complex, obtained as a result of the EXAFS analysis, are presented in Table 2. The full version of these data for all four coordination spheres for the studied samples is presented in Table S2 (ESI<sup>†</sup>). From the data in Table 2, we can see that when using the monomer model for fitting, the interatomic distances  $R(\text{Ni–O})$  and  $R(\text{Ni–N})$  were considered to be equal, and their values were  $1.851 \pm 0.006$  Å. However, in the case of the d–d dimer model, these distances are different and amount to  $1.89 \pm 0.04$  and  $1.84 \pm 0.03$  Å,

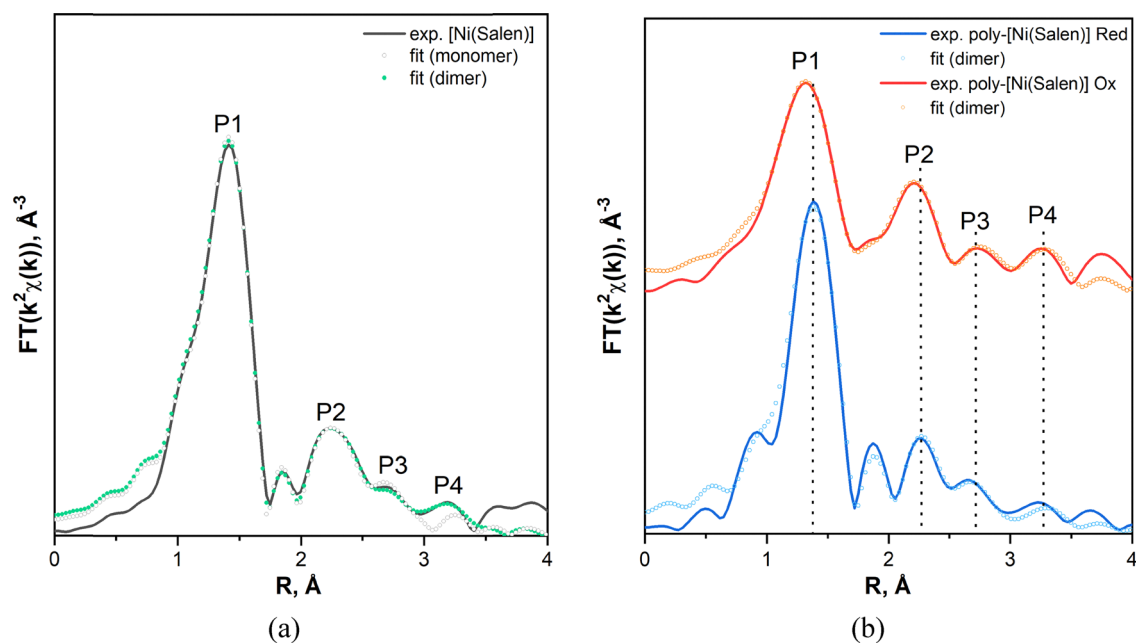


Fig. 6 (a) Fourier transforms of the experimental Ni 1s EXAFS  $k^2\chi(k)$  signals for  $[\text{Ni}(\text{Salen})]$ : the black solid line is experimental EXAFS data, and black open and green solid circles are simulated fitting curves for the structure of the monomer and dimer, respectively. (b) Fourier transforms of the experimental Ni 1s EXAFS  $k^2\chi(k)$  signals for poly- $[\text{Ni}(\text{Salen})]$ -Ox and poly- $[\text{Ni}(\text{Salen})]$ -Red: solid (blue and red) lines are experimental EXAFS data and open circles are simulated fitting curves.

**Table 2** Structural parameters for the first and fourth coordination spheres obtained from modeling FT curves of Ni 1s EXAFS spectra of the [Ni(Salen)] complex and its polymer in Red as well as Ox charged states

Sample	Scattering path	<i>N</i>	<i>R</i> , Å	$\sigma^2$ , Å <sup>2</sup>	<i>R<sub>f</sub></i> , %
[Ni(Salen)] (model monomer)	P1 Ni–N, Ni–O	4	1.851 ± 0.006	0.0020	0.6
	P4 Ni–C1	4	3.21 ± 0.03	0.0045	
[Ni(Salen)] (model d–d dimer)	P1 Ni–N	2	1.84 ± 0.03	0.0023	0.14
	Ni–O	2	1.89 ± 0.04		
	P4 Ni–Ni	1	3.64 ± 0.04	0.0107	
	Ni–N–O	4	3.73 ± 0.04	0.0085	
Poly-[Ni(Salen)]-Ox (model d–d dimer)	P1 Ni–N	2	1.798 ± 0.006	0.0014	0.17
	Ni–O	2	1.967 ± 0.011		
	P4 Ni–Ni	1	3.566 ± 0.014	0.0022	
	Ni–O–N	2	3.484 ± 0.048	0.0063	
Poly-[Ni(Salen)]-Red (model d–d dimer)	P1 Ni–N	2	1.854 ± 0.021	0.0011	1.09
	Ni–O	2	1.865 ± 0.020		
	P4 Ni–Ni	1	3.560 ± 0.049	0.0059	
	Ni–O–N	4	3.659 ± 0.214	0.017	

*N* – Coordination number (for multiple scattering paths of the photoelectron – degeneracy multiplicity), *R* – Interatomic distance,  $\sigma^2$  – Debye-Waller factor, *R<sub>f</sub>* – *R*-factor characterizing the quality of modeled fit of experimental EXAFS oscillations.

respectively. In addition, using the dimer model, we were also able to well approximate the P4 band observed in the FT curve of the EXAFS spectrum, attributing it predominantly to Ni–Ni single scattering, and determine the interatomic distance *R*(Ni–Ni) between neighboring monomers, which was 3.64 ± 0.04 Å, whereas, in the case of the monomer model, the contributions from C1 atoms give only a very weak band at *R* ~ 3.2 Å, which does not coincide with the P4 band on the experimental curve (see Fig. 6a). Analyzing the data in Fig. 6a, it should be noted that the theoretical model for a centrosymmetric d–d dimer consisting of two monomeric fragments best matches the experimental spectrum of the [Ni(Salen)] complex. The *R*-factor (*R<sub>f</sub>*) characterizing the quality of modeled fit of experimental EXAFS oscillations for this model is 0.14%, which indicates a good fit. It is also important to note that, in general, the determined *R*(Ni–O), *R*(Ni–N), and *R*(Ni–Ni) distances from the EXAFS analysis coincide quite well with the data obtained from the DFT calculation (see Tables 1 and 2). Therefore, the structure of the [Ni(Salen)] complex in the condensed state can be described by the d–d dimer model.

To describe the FT curves of the experimental EXAFS spectra, the polymer, dimer and tetramer models were used. However, during the preliminary procedures of EXAFS data fitting, it was found that the use of tetramer models leads to high *R<sub>f</sub>* values. Considering that the tetramer is composed of two dimer fragments linked by a C–C bond, in order to simplify the fitting, it was decided to use only the d–d dimer model to determine the structural parameters of poly-[Ni(Salen)] both in the reduced and oxidized charge states (Fig. 6b). The suitability of this approach is confirmed by the low *R<sub>f</sub>* values, which were 0.17% for poly-[Ni(Salen)]-Ox and 1.09% for poly-[Ni(Salen)]-Red (Table 2).

From the approximation data presented in Table 2 it can be seen that the number of atoms in the first coordination sphere (P1) remains equal to four on going from the complex to the polymer. The main changes are observed in the interatomic distances *R*(Ni–O) and *R*(Ni–N) of the [NiO<sub>2</sub>N<sub>2</sub>] coordination center. In the case of the poly-[Ni(Salen)]-Ox, the values of *R*(Ni–O) increase from 1.89 ± 0.04 to 1.967 ± 0.011 Å, while those of *R*(Ni–N), in contrast, decrease from 1.84 ± 0.03 to

1.798 ± 0.006 Å compared to the complex. This result clearly indicates that during the electrochemical oxidation process, the square-planar structure of the [NiO<sub>2</sub>N<sub>2</sub>] coordination center in the dimeric fragments of the complex becomes distorted. This distortion is most probably caused by the phenolate–quinone transformation of the ligand. It should be noted that information obtained regarding the geometry of the coordination center for poly-[Ni(Salen)]-Ox contradicts the widely accepted conclusion that electropolymerization and oxidation of salen-based conjugated polymers do not cause significant changes in the local structure around the metal atom.<sup>27,30,35</sup> At the same time, for poly-[Ni(Salen)]-Red, the interatomic distances *R*(Ni–O) and *R*(Ni–N) are 1.865 ± 0.020 and 1.854 ± 0.021 Å, which are quite close to the values obtained for the [Ni(Salen)] complex (1.89 ± 0.04 and 1.84 ± 0.03 Å). Therefore, it is logical to conclude that the geometric structure of the coordination center upon moving from the oxidized to the neutral (reduced) state of the polymer is practically restored to a square-planar one. It is also worth noting that the *R*(Ni–Ni) distances between nickel atoms in the dimers, which were obtained by analyzing the P4 scattering paths, were slightly different for the complex and the polymer in both states, amounting to 3.64 ± 0.04 Å and 3.566 ± 0.014 Å (Ox state) and 3.560 ± 0.049 Å (Red state), respectively (Table 2). In other words, during the process of electrochemical oxidation, the monomers in the dimers come closer to each other. At the same time, there are practically no differences between the oxidized and reduced charge states.

It is also noteworthy that the *R*(Ni–O), *R*(Ni–N), and *R*(Ni–Ni) interatomic distances determined using EXAFS for poly-[Ni(Salen)]-Red generally correlate with the DFT data for the tetramer structure with *q* = 0 (Tables 1 and 2). The DFT data show slightly lower values for *R*(Ni–O) and *R*(Ni–Ni). However, for poly-[Ni(Salen)]-Ox, when using the tetramer structures with *q* = +3 and +3 with the BF<sub>4</sub><sup>–</sup> counterion, the DFT data diverge from the EXAFS results, but in general the same trend towards increasing distortions of the coordination center geometry is observed. At the same time, the lower values of *R*(Ni–Ni) obtained in the DFT calculations for tetramers relative to the

EXAFS data for the corresponding charge states of the polymer can be explained by the limitations of the models used, which consider only one structural unit of the polymer.

### 3.3. NEXAFS

Now, let us move on to examining the experimental Ni 1s NEXAFS spectra of the [Ni(Salen)] complex and its polymer in different charge states, which are presented in Fig. 7. The designations of the absorption structures in these spectra are consistent with those in the Ni 2p spectrum of the [Ni(Salen)] complex reported in our previous study.<sup>36</sup> For further discussion, we also show the Ni 1s absorption spectrum of nickel oxide NiO here. The spectra of the complex and polymer are characterized in the vicinity of the Ni 1s edge by a similar fine structure, which is formed by absorption bands (resonances) A, C, D, E, and F, as well as a much broader band G, having close energy positions in the spectra compared and differing mainly in their relative intensities and contrast. These differences in the Ni 1s NEXAFS spectra are most clearly seen in moving from the monomer to the polymer in the oxidized state, poly-[Ni(Salen)]-Ox. The subsequent transition to the polymer in a reduced state, poly-[Ni(Salen)]-Red, largely returns the Ni 1s spectrum to its original shape of the monomer spectrum. Thus, it is clear that these differences in the compared Ni 1s NEXAFS spectra reflect changes in the atomic structure of the [Ni(Salen)] complex. These structural changes are caused by the coupling of monomers during their electrochemical polymerization.

As is known,<sup>20</sup> absorption resonances in NEXAFS spectra can be treated as a result of transitions of core electrons to unoccupied MOs of the quasi-molecule formed by the absorbing atom and the atoms of its nearest surroundings. In our case, the role of such a quasi-molecule is played by the [NiO<sub>2</sub>N<sub>2</sub>] coordination center of the [Ni(Salen)] complex and, therefore, the fine structure of the Ni 1s absorption spectra of this complex and its polymers is dominated by dipole-allowed transitions of the Ni 1s electrons to unoccupied MOs, which contain contributions of 4p electron states of the nickel atom. Considering that the coordination center of [NiO<sub>2</sub>N<sub>2</sub>] is an almost square-planar quasi-molecule,<sup>36</sup> it can be argued that the vacant electronic states, achieved by dipole absorption transitions of Ni 1s electrons, are described by  $\pi$ - and  $\sigma$ -type MOs with the Ni 4p<sub>z</sub> and Ni 4p<sub>x,y</sub> contributions, respectively. It is well known that the lower energy MOs correspond to the  $\pi$  states, while the  $\sigma$  states are responsible for the MOs at higher energies. Thus, it is obvious that the intense absorption bands C and D, E, and F in the spectra under consideration are associated with dipole transitions of Ni 1s electrons to  $\pi$ - and  $\sigma$ -type MOs, respectively. These resonances are located at photon energies of  $\sim 8338$  eV (C),  $\sim 8349$  eV (D),  $\sim 8359$  eV (E), and  $\sim 8375$  eV (F) and, as noted above, are most clearly visible in the Ni 1s spectrum of the monomeric [Ni(Salen)] complex. It should also be noted that in all spectra a low-intensity absorption band A is also observed at the lowest photon energy of  $\sim 8333$  eV (Fig. 7, inset). As will be shown below, it is associated with quadrupole Ni 1s  $\rightarrow$  3d transitions, characteristic of square-planar nickel(II) complexes.<sup>56</sup>

The Ni atom in the [Ni(Salen)] complex has a formal valence electron configuration of the Ni<sup>2+</sup> cation, [Ne]3s<sup>2</sup>3p<sup>6</sup>3d<sup>8</sup>,

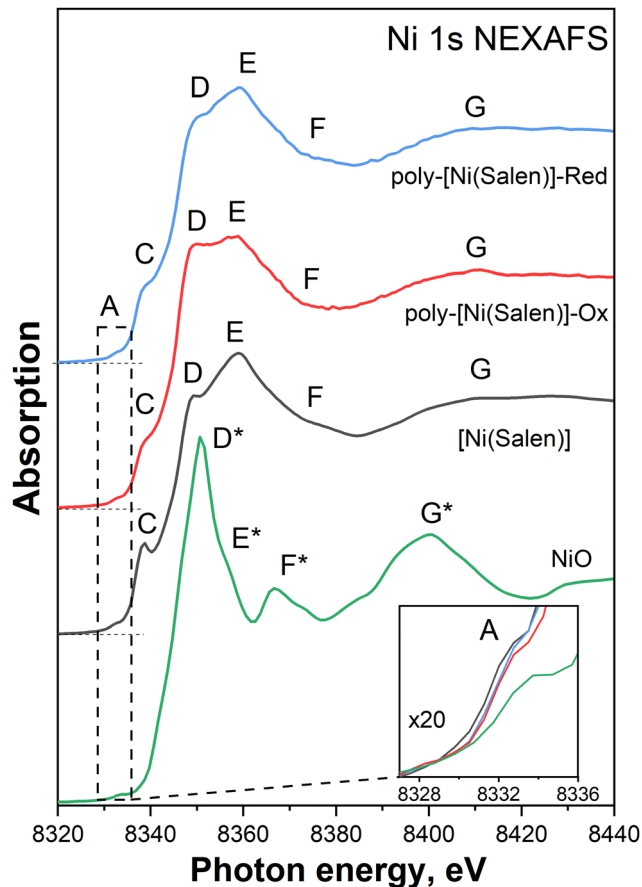


Fig. 7 Ni 1s NEXAFS spectra of the [Ni(Salen)] complex and its polymer in different charge states as well as the spectrum of the reference NiO compound. The intensity of absorption structures in the compared spectra is normalized to that of the continuous absorption jump at a photon energy of 8440 eV. In the inset, the absorption band A in the spectra of different objects is presented on an enlarged scale.

characteristic of Ni(II) compounds. The covalent bonding of the Ni atom with the oxygen and nitrogen atoms in the [NiO<sub>2</sub>N<sub>2</sub>] coordination center has a donor-acceptor nature and is realized by displacing the lone 2p electron pairs of the O and N atoms to the empty 3d orbital of the nickel atom.<sup>57</sup> As a result, four sp<sup>2</sup>d hybridized  $\sigma$  bonds are formed for the nickel atom with the participation of Ni 4s, 4p, and 3d AOs, which provide square-planar coordination of the Ni atom by O and N atoms with close interatomic distances  $R(\text{Ni-O}) = 1.882$  Å and  $R(\text{Ni-N}) = 1.889$  Å.<sup>53</sup>

The energy spectrum of the [NiO<sub>2</sub>N<sub>2</sub>] coordination center can be described using the spectral distribution of the bonding, nonbonding and antibonding one-electron MOs of this system. In the case of a square-planar molecule (symmetry group  $D_{4h}$ ), these MOs are differently oriented with respect to the molecular plane:  $\sigma$ -type MOs are arranged in the plane and  $\pi$ -type MOs are perpendicular to it. In the NiO<sub>2</sub>N<sub>2</sub> quasi-molecule, the Ni 3d AOs are mixed with O and N 2p-AOs forming  $\sigma$ -type MOs –  $a_{1g}$  and  $b_{1g}$  and  $\pi$ -type MOs –  $b_{2g}$  and  $e_g$ . The Ni 4s AO also contributes to the  $\sigma_{a_{1g}}$  MO. If we take into account that Ni 4p AOs also participate in the chemical bonding of the nickel

atom with oxygen and nitrogen atoms, this leads to the formation of  $\sigma_{e_u}$ ,  $\pi a_{2u}$  and  $\pi e_u$  MOs. It is also worth noting that two more  $\pi$ -type MOs,  $a_{2g}$  and  $b_{2u}$ , are formed from O and N 2p AOs and are nonbonding.<sup>57</sup>

When identifying the Ni 1s NEXAFS spectrum of [Ni(Salen)], we must first take into account the dipole-allowed transitions of Ni 1s electrons to unoccupied MOs of the [NiO<sub>2</sub>N<sub>2</sub>] coordination center with contributions of Ni 4p AOs, *i.e.*  $\sigma_{e_u}$ ,  $\pi a_{2u}$  and  $\pi e_u$ -MOs. In this case, the narrow peak C in its shape and energy position corresponds to transitions of Ni 1s electrons to the unoccupied antibonding  $\pi a_{2u}$ -MO originating from the Ni 4p<sub>z</sub> AO, whereas the broad and intense absorption band with the D and E components is probably associated with electron transitions to the antibonding  $\sigma_{e_u}$ -MO with Ni 4p<sub>x,y</sub> contributions. Since the real C<sub>2v</sub> symmetry group of the [NiO<sub>2</sub>N<sub>2</sub>] coordination center is lower than the above-considered D<sub>4h</sub> symmetry group, it is obvious that the doubly degenerate  $\sigma_{e_u}$ (Ni 4p<sub>x,y</sub>)-MO will split into two non-degenerate  $\sigma_{b_1}$ (Ni 4p<sub>x</sub>)- and  $\sigma_{b_2}$ (Ni 4p<sub>y</sub>)-MOs.<sup>57</sup> Therefore, it is logical to assert that these D and E components in the Ni 1s NEXAFS spectrum of [Ni(Salen)] are due to the transitions of the Ni 1s electrons to the  $\sigma_{b_1}$ - and  $\sigma_{b_2}$ -MOs of the [NiO<sub>2</sub>N<sub>2</sub>] coordination center. Taking into account the above-mentioned relationship between absorption bands and multiple scattering resonances of Ni 1s photoelectrons by atoms of the nearest surroundings (oxygen and nitrogen), it can also be argued that the antibonding  $\sigma_{b_1}$ - and  $\sigma_{b_2}$ -MOs mainly characterize the  $\sigma$ (Ni–N) and  $\sigma$ (Ni–O) covalent bonds, respectively. Since the *R*(Ni–O) interatomic distance is shorter than the *R*(Ni–N) one, the resonance associated with the photoelectron scattering by oxygen atoms should be at a higher photoelectron energy.<sup>19</sup> In this case, the higher intensity of the E band compared to that of the D band reflects the higher scattering power for oxygen atoms compared to nitrogen atoms.

Here it seems instructive to compare the spectrum of [Ni(Salen)] with that of NiO (Fig. 7). In the oxide, the Ni atom has a more symmetrical nearest surrounding in the form of an octahedral NiO<sub>6</sub> quasi-molecule, the 4p AOs of which are completely degenerate. These orbitals, along with Ni 4s and 3d AOs, determine the octahedral atomic structure of the NiO<sub>6</sub> quasi-molecule. They form six sp<sup>3</sup>d<sup>2</sup> hybridized  $\sigma$  bonds, which are characterized by  $\sigma$ -MOs of a<sub>1g</sub>(Ni 4s), t<sub>1u</sub>(Ni 4p) and e<sub>g</sub>(Ni 3d) symmetry types.<sup>57</sup> As can be seen in Fig. 7, the NiO spectrum is dominated by an intense absorption resonance D\* with a high-energy shoulder E\* and a less intense F\* band. From the above, it is obvious that the D\* resonance is due to the transitions of Ni 1s electrons to the empty antibonding  $\sigma_{t_{1u}}$ -MO of the octahedral NiO<sub>6</sub> quasi-molecule, which is formed by the Ni 4p AOs. This resonance, which is a counterpart of the E band in the [Ni(Salen)] spectrum and corresponds to the resonant scattering of Ni 1s photoelectrons by oxygen atoms, is observed at the photoelectron energy that is approximately 8 eV lower than in the complex spectrum. This is due to the fact the interatomic distance in the oxide, *R*(Ni–O) = 2.085 Å,<sup>58</sup> is noticeably greater than this distance in the complex (1.882 Å<sup>53</sup>). The appearance of the E\* shoulder is likely associated with the splitting of the absorption Ni 1s →  $\sigma_{t_{1u}}$ (Ni 4p)-MO transition due to a slight distortion of the

octahedral surroundings of the nickel atom in the oxide. Due to the absence of significant splitting of the Ni 4p AOs in the NiO<sub>6</sub> quasi-molecule, the counterpart of the C band in the complex spectrum is not observed in the spectrum of NiO, but a low-intensity lowest-energy band A remains.

Let us now compare the Ni 1s NEXAFS spectra of the [Ni(Salen)] monomer complex and its poly-[Ni(Salen)] polymer in various charge states, as shown in Fig. 7. As mentioned above, the Ni 1s absorption spectra of the polymer contain bands A, C, D, E, and F and a broad G band, as in the spectrum of the monomer complex. Moreover, the energy positions of the corresponding bands coincide quite well in the compared spectra. The presence of bands A and C in the spectra of the polymer, both in the oxidized and reduced states, clearly indicates the maintenance of the square-planar structure of the [NiO<sub>2</sub>N<sub>2</sub>] coordination center during the polymerization process of the complex. However, there are some differences between the spectra of the polymer in different charge states and also when compared to the spectrum of the monomer. In particular, the C–E bands in the polymer spectra are smeared and less distinct compared to the monomer spectrum, which is especially noticeable in the spectrum of the oxidized polymer. In addition, there is a significant difference between the spectra of the polymer and its monomer complex in the relative intensities of the D and E bands, which characterize the  $\sigma$ (Ni–N) and  $\sigma$ (Ni–O) bonding in the [NiO<sub>2</sub>N<sub>2</sub>] coordination center. In other words, this finding confirms the change in the interatomic *R*(Ni–N) and *R*(Ni–O) distances when moving from the complex to its polymer, as was also detected through the analysis of EXAFS spectra (Table 2).

To definitively identify the structural fragments that are responsible for the basic properties of the [Ni(Salen)] complex and its polymer in both the reduced and oxidized states we compared the modelled Ni 1s NEXAFS spectra for the monomer and dimer structures, as well as for the tetramer structures with a different total charge *q* equal to 0, +3, and +3 (with the BF<sub>4</sub><sup>−</sup> counterion) with the experimental spectra (Fig. 8). For this purpose, the theoretical Ni 1s spectra were energetically aligned with the experimental ones by adjusting the calculated Fermi level until the energy position of the C band in the compared spectra matched. It should be noted that the A band is not present in the calculated Ni 1s spectra of all models, since only dipole transitions of Ni 1s electrons to unoccupied MOs with Ni 4p AO contributions were considered in the calculations.

In Fig. 8a, the experimental Ni 1s NEXAFS spectrum of the [Ni(Salen)] complex (black curve) is compared to the simulated spectra of the monomer (red curve) and dimer (blue curve) structures. It is clear that the experimental Ni 1s spectrum and the compared one of the monomer model are very similar in terms of the overall spectral behavior, as well as the number and energy position of the absorption bands. The most noticeable differences between the simulated spectrum for the monomer model and the experimental data are a significant reduction in contrast and a lack of clear peaks for the C and D bands. In this case, there is only one E band with a clear maximum. However, when comparing the theoretical spectrum

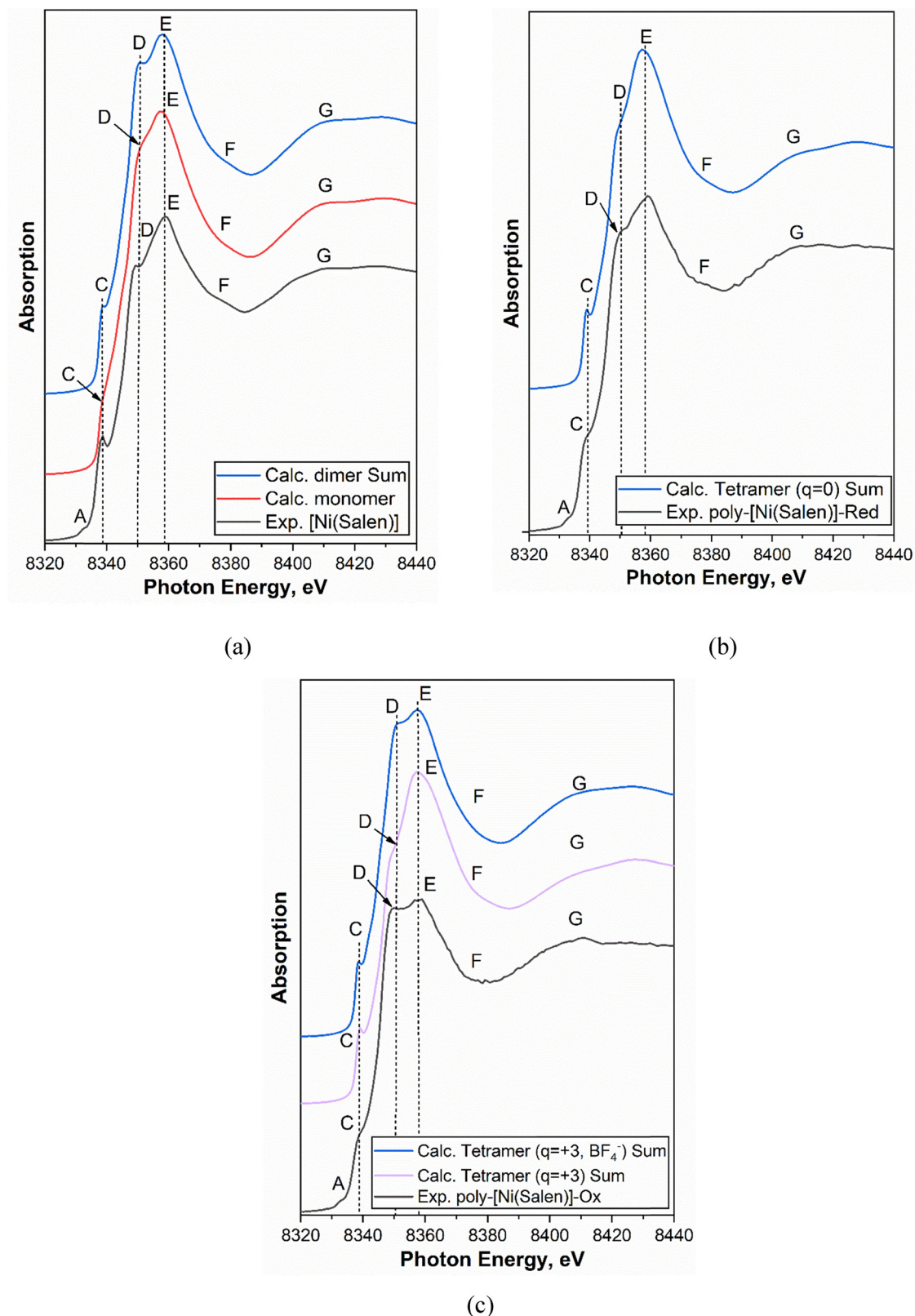


Fig. 8 Experimental Ni 1s NEXAFS spectra of the (a) [Ni(Salen)], (b) poly-[Ni(Salen)]-Red, (c) poly-[Ni(Salen)]-Ox, and simulated spectra of the model structures (monomer, d-d dimer and tetramer with different total charges ( $q$ ): 0, +3, and +3(with the  $\text{BF}_4^-$  counterion)).

of the monomer and dimer, it is seen that the C and D bands are well resolved in the spectrum of the latter as in the

experimental spectrum. In addition, the simulated Ni 1s spectrum of the dimer model more closely matches the experimental

spectrum, especially in the region of the D and E absorption bands characterizing  $\sigma(\text{Ni-N})$  and  $\sigma(\text{Ni-O})$  bonding in the  $[\text{NiO}_2\text{N}_2]$  coordination center. Therefore, it can be argued that the structure and properties of the  $[\text{Ni}(\text{Salen})]$  complex in the condensed state is best described by centrosymmetric d-d dimer fragments.

Now, let us compare the experimental Ni 1s NEXAFS spectrum of the poly- $[\text{Ni}(\text{Salen})]$ -Red polymer (black curve) with the theoretical one of a tetramer with a total charge  $q = 0$  (blue curve), shown in Fig. 8b. It should be noted that the theoretical spectrum was obtained by summing the simulated Ni 1s spectra of each of the four Ni atoms of the monomer fragments included in the tetramer structure. In general, the compared theoretical Ni 1s NEXAFS spectrum is similar to the experimental spectrum of the polymer in the reduced state in the number and energy position of the main absorption bands. In addition, the spectral behavior in the region of the C-E bands, which characterize the unoccupied MOs with Ni 4p AOs contributions for the  $[\text{NiO}_2\text{N}_2]$  coordination center, is similar for both spectra. These observations allow us to conclude that the proposed model of a tetramer with a total charge of 0 accurately describes the basic properties of the poly- $[\text{Ni}(\text{Salen})]$  polymer in its reduced state.

Finally, we will discuss the experimental Ni 1s NEXAFS spectrum of poly- $[\text{Ni}(\text{Salen})]$ -Ox (black curve) and the theoretical spectra (purple and blue curves) for tetramers with total charges of +3 and +3 (with the  $\text{BF}_4^-$  counterion), which are shown in Fig. 8c. Comparing these spectra, we can see that the fine structure of the experimental Ni 1s spectrum of poly- $[\text{Ni}(\text{Salen})]$ -Ox closely matches the structure of the simulated spectrum only for the  $\text{BF}_4^-$  doped tetramer with  $q = +3$ , especially in the region of the D and E bands. Based on this, we can conclude that the tetramer with a total charge of +3 and the  $\text{BF}_4^-$  counterion can be considered as a structural fragment that determines the basic properties of the polymer in an oxidized state.

To obtain more complete information about the spectrum and properties of lower unoccupied MOs for the  $[\text{NiO}_2\text{N}_2]$  coordination center, we now consider the fine structure of the Ni 1s NEXAFS spectrum of  $[\text{Ni}(\text{Salen})]$  simultaneously with that of the Ni  $2p_{3/2}$  spectrum, which was previously interpreted

within the framework of the quasi-molecular  $\text{NiO}_2\text{N}_2$  approach.<sup>36</sup> To do this, we energetically align the Ni 1s NEXAFS spectrum of the complex with its Ni  $2p_{3/2}$  spectrum, using the energy difference between the 1s and  $2p_{3/2}$  core levels of the Ni atom in the complex, which is equal to the photon energy of the characteristic Ni  $K\alpha_1$  ( $1s \rightarrow 2p_{3/2}$ ) line for the  $[\text{Ni}(\text{Salen})]$  complex. According to data,<sup>59</sup> it practically coincides with the photon energy of this line for metallic nickel and is equal to 7478.15 eV.<sup>60</sup> A similar approach was also used to construct the energetically aligned Ni  $2p_{3/2}$  and Ni 1s spectra of the polymer in the oxidized and reduced states.

The energetically aligned Ni 1s and  $2p_{3/2}$  NEXAFS spectra of the  $[\text{Ni}(\text{Salen})]$  complex are shown in Fig. 9a. When examining these spectra, it becomes clear that the lowest-energy resonance A and absorption band C in the Ni 1s spectrum have counterparts A and C in the Ni  $2p_{3/2}$  spectrum, which coincide well in their energy positions, but differ significantly in their relative intensities. A small deviation of approximately 0.9 eV in the energy positions of band C observed between Ni 1s and  $2p_{3/2}$  NEXAFS spectra of  $[\text{Ni}(\text{Salen})]$  can naturally be attributed to the different effect of the corresponding core holes on the energy position of unoccupied electronic states. This final-state effect occurs due to Coulomb and exchange interactions between an inner-shell vacancy and an electron promoted to an empty state. Depending on the specific electron vacancy in a molecule, this results in a different energy position for the core electron excitation relative to the vacuum level, usually within about 1 eV, in the corresponding spectra.<sup>20</sup>

It has been shown above that the antibonding  $\pi_{a_{2u}}$  MO, originating from the Ni  $4p_z$  AO, is responsible for the C band in the Ni 1s NEXAFS spectrum of the  $[\text{Ni}(\text{Salen})]$  complex. However, the actual symmetry group of the  $[\text{NiO}_2\text{N}_2]$  coordination center is the  $C_{2v}$  symmetry group, which is less symmetric than the  $D_{4h}$  group used. As a result of this decrease in the symmetry of the coordination center, the Ni 4p AOs will be mixed with the 3d AOs and the considered antibonding  $\pi$  MO will get an additional contribution from the Ni 3d AOs. The presence of the C band in the Ni  $2p_{3/2}$  spectrum is directly related to this Ni 3d contribution in the considered MO.

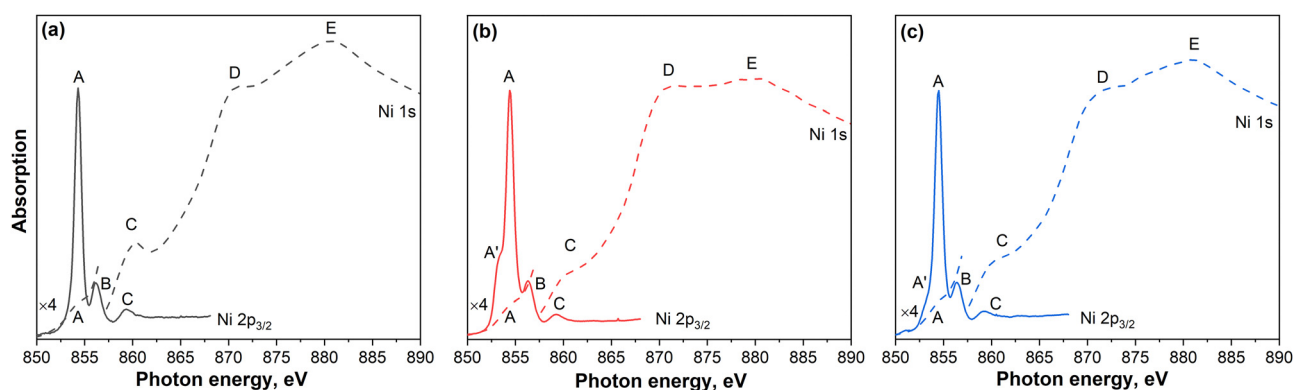


Fig. 9 Energetically aligned Ni  $2p_{3/2}$ - and Ni 1s absorption spectra of the  $[\text{Ni}(\text{Salen})]$  complex (a) and its polymer in Ox (b) and Red (c) charge states. The Ni 1s spectra are referred to the scale of the Ni  $2p_{3/2}$  spectra using the photon energy of the characteristic  $K\alpha_1(1s \rightarrow 2p_{3/2})$  line for the  $[\text{Ni}(\text{Salen})]$  complex (7478.15 eV).<sup>59</sup>

The A band, in turn, is explained by transitions of Ni  $2p_{3/2}$  electrons to the lowest unoccupied electronic state of  $[\text{NiO}_2\text{N}_2]$ , which, within the framework of the  $D_{4h}$  symmetry, is described as a weakly antibonding  $\sigma b_{1g}$  MO with a dominant contribution from Ni  $3d\sigma$  AOs.<sup>36</sup> It should be noted that the very low intensity of the A band in the Ni 1s spectrum compared to the Ni  $2p_{3/2}$  spectrum is due to the quadrupole character of the Ni  $1s \rightarrow \sigma b_{1g}$  (Ni  $3d\sigma$  AO) MO electronic transitions. The remaining absorption bands in the compared spectra are the result of dipole transitions, such as the Ni  $1s \rightarrow \pi a_{2u}$  (Ni  $4p_z\pi + \text{Ni } 3d\pi$  AO) MO for band C in the Ni 1s spectrum and Ni  $2p_{3/2} \rightarrow \sigma b_{1g}$  (Ni  $3d\sigma$ ) MO and Ni  $2p_{3/2} \rightarrow \pi a_{2u}$  (Ni  $3d\pi$ ) MO for bands A and C in the Ni  $2p_{3/2}$  spectrum. Thus, this finding clearly indicates that the bands A and C in the Ni 1s spectrum are caused by 1s electron transitions to the same unoccupied MOs that are responsible for these bands in the  $2p_{3/2}$  spectrum.

At the same time, an additional absorption band B is observed in the Ni  $2p_{3/2}$  spectrum. As shown in ref. 36, it is caused by the  $2p_{3/2}$  electron transition to the  $\pi e_g$  (Ni  $3d$ ) MO, which also manifests as an intense absorption resonance in the 1s NEXAFS spectra of oxygen and nitrogen atoms. This  $e_g$  MO is formed as a result of the covalent mixing of the N and O  $2p\pi$  AOs and Ni  $3d_{xz,yz}\pi$  orbitals and reflects the presence of additional  $\pi$  bonding between the complexing Ni atom and the N and O ligand atoms in the  $[\text{NiO}_2\text{N}_2]$  coordination center. This bonding is accompanied by the charge transfer from the Ni atom to the ligand atoms, also known as the “ $\pi$ -back donation” effect. The counterparts of the D and E bands are not observed in the Ni  $2p_{3/2}$  spectrum, as they overlap with the Ni  $2p_{1/2}$  spectrum.

A comparison of the Ni  $2p_{3/2}$  spectra of the  $[\text{Ni}(\text{Salen})]$  complex and the poly- $[\text{Ni}(\text{Salen})]$  polymer, in both charge states, reveals that they are similar in the overall spectral behavior, the number of main absorption bands and their energy positions (Fig. 9). However, there are significant differences between the spectra of the polymer in different charge states and also when compared to the spectrum of the monomer. A detailed examination of the Ni  $2p_{3/2}$  spectra of the polymer reveals an additional absorption band A' in the region of lower photon energies, which is not present in the spectrum of the complex. Interestingly, this band shows a higher intensity in the spectrum of the oxidized polymer compared to the reduced one. Thus, the observed differences in the Ni  $2p_{3/2}$  spectra of the polymer depend on its charge state, which is related to the number of  $\text{BF}_4^-$  counterions adsorbed in the near-surface layer of the polymer. Obviously, these counterions can interact with atoms of the  $[\text{NiO}_2\text{N}_2]$  coordination centers of the monomer involved in the polymerization process. It is reasonable to assume that this interaction will result in a change in the interatomic distances and effective charges of the atoms in these coordination centers. In this case, a small transfer of electron density from the  $\text{BF}_4^-$  counterion to the complexing cation  $\text{Ni}^{2+}$  will lead to a decrease in its effective positive charge and, as a result, a small low-energy shift in resonance A and the appearance of the A' band. Thus, the new absorption band A' is caused by transitions of Ni 1s electrons to

the  $\sigma b_{1g}$  MO localized on Ni atoms with a reduced effective charge. It is crucial that the Ni 1s electron transition responsible for the A' band is identical to that for the A band. As mentioned above, band A' is the most intense in the Ni 1s spectrum of the oxidized polymer and becomes noticeably weaker in that of the reduced polymer, although it does not disappear completely. This suggests that the counterions are only partially returned to the electrolyte during the reduction reaction.

Based on the comparative analysis of the Ni 1s NEXAFS spectrum and the previously identified the Ni  $2p_{3/2}$  spectrum of the complex,<sup>36</sup> it can be argued that the local electronic structure of the coordination center  $[\text{NiO}_2\text{N}_2]$  in the monomeric complex is determined within the framework of square-planar symmetry ( $D_{4h}$ ) by the sequence of vacant antibonding MOs formed by Ni-AOs, namely:  $\sigma b_{1g}(\text{Ni } 3d_{yz})$  – band A,  $\pi e_g(\text{Ni } 3d_{xz,yz})$  – band B,  $\pi a_{2u}(\text{Ni } 4p_z)$  – band C and  $\sigma e_u(\text{Ni } 4p_{x,y})$  – bands D and E. Considering the decrease in symmetry from  $D_{4h}$  to  $C_{2v}$  for  $[\text{NiO}_2\text{N}_2]$ , the Ni 4p and 3d AOs are mixed, and the doubly degenerate  $e_g$  and  $e_u$  MOs are split into nondegenerate  $b_1$  and  $b_2$ . These changes in symmetry account for the presence of the bands C, D, and E in the Ni 1s NEXAFS spectrum of the complex. For the case of the polymer in both the oxidized and reduced states, the local electronic structure of the coordination center is described by the same sequence of vacant antibonding MOs as for the complex.

## 4. Conclusions

The atomic-electronic structure of the  $[\text{NiO}_2\text{N}_2]$  coordination center of the  $[\text{Ni}(\text{Salen})]$  complex and its polymer was studied based on a detailed examination of the Ni 1s EXAFS and Ni 1s(2p) NEXAFS spectra of these materials that was supplemented by quantum chemical calculations.

At the first stage, DFT calculations were used to construct initial models of the  $[\text{Ni}(\text{Salen})]$  complex in the condensed state, as well as to find the structural units (fragments) of its polymer that determine the basic properties of the polymer in the reduced and oxidized states. In the case of the complex, the structures were a monomer and a d-d dimer, whereas in the case of the polymer, tetramers were constructed from two cross-linked d-d dimers, which were optimized at different total charges of 0, +1, +2, +3, +3 (with the  $\text{BF}_4^-$  counterion) and +4. Based on the analysis of the Ni 1s EXAFS spectra, it has been shown that the d-d dimer model provides the best description of the structure and properties of the complex in the condensed state. In addition, it has also been discovered that the d-d dimer can serve as a simplified model for polymers. It has been established that during the transition from the complex to the polymer, the planar structure of the  $[\text{NiO}_2\text{N}_2]$  coordination center of the monomers remains unchanged. However, upon the oxidation of monomer molecules, the atomic structure of the coordination center is distorted, as shown by a change in the interatomic  $R(\text{Ni}-\text{O})$  and  $R(\text{Ni}-\text{N})$  distances from  $1.89 \pm 0.04$  to  $1.967 \pm 0.011$  Å and from  $1.84 \pm 0.03$  to  $1.798 \pm 0.006$  Å,

respectively, compared to the complex. This distortion is most probably caused by the phenolate–quinone transformation of the ligand. At the same time, upon moving from the oxidized to the neutral (reduced) state of the polymer, the atomic structure of the  $[\text{NiO}_2\text{N}_2]$  coordination center is almost restored to a square-planar one: the interatomic distances  $R(\text{Ni}-\text{O})$  and  $R(\text{Ni}-\text{N})$  become equal to  $1.865 \pm 0.020$  and  $1.854 \pm 0.021$  Å.

The empirical identification of the absorption bands of the Ni 1s NEXAFS spectra of the complex and its polymer was carried out within the framework of a quasi-molecular  $\text{NiO}_2\text{N}_2$  analysis, and the main absorption bands were attributed to Ni 1s electron transitions to vacant MOs of this quasi-molecule. Then the experimental Ni 1s NEXAFS spectra were compared with the simulated ones for the final selection of the structural fragments responsible for the basic properties of the  $[\text{Ni}(\text{Salen})]$  complex and its polymer, both in reduced and oxidized states. It has been found that the structural unit that describes the properties of a molecular complex in the condensed state is a d–d stacked dimer. In the case of the polymer in the reduced and oxidized states, these structures are tetramers formed by cross-linking d–d dimers, with a total charge of 0 and +3 (with the  $\text{BF}_4^-$  counterion), respectively.

A joint analysis of the Ni 1s and  $2p_{3/2}$  NEXAFS spectra has allowed us to establish that the local electronic structure of the square-planar  $[\text{NiO}_2\text{N}_2]$  coordination center in the complex, within the framework of the  $D_{4h}$  symmetry, can be characterized by the sequence of vacant antibonding MOs formed by Ni AO:  $\sigma_{b_{1g}}(\text{Ni } 3d_{yz})$ ,  $\pi_{e_g}(\text{Ni } 3d_{xz,yz})$ ,  $\pi_{a_{2u}}(\text{Ni } 4p_z)$  and  $\sigma_{e_u}(\text{Ni } 4p_{x,y})$ . However, due to the decrease in the actual symmetry of the  $[\text{NiO}_2\text{N}_2]$  coordination center in the polymer from  $D_{4h}$  to  $C_{2v}$ , the Ni 4p and 3d AOs are mixed, and doubly degenerate  $e_g$  and  $e_u$  MOs are split into nondegenerate  $b_1$  and  $b_2$  orbitals. Thus, the local electronic structure of the coordination center for poly- $[\text{Ni}(\text{Salen})]$ -Red can also be described by the same set of antibonding MOs as for the monomer complex. The appearance of a new low-energy band A' in the Ni  $2p_{3/2}$  spectrum of poly- $[\text{Ni}(\text{Salen})]$ -Ox is due to the transitions of Ni  $2p_{3/2}$  electrons to  $\sigma_{b_{1g}}$  MOs, which are localized on Ni atoms with a reduced effective charge due to the interaction between the Ni atom and  $\text{BF}_4^-$  counterions.

## Author contributions

The manuscript was written through contributions of all authors. All authors have given approval to the final version of the manuscript.

## Conflicts of interest

There are no conflicts to declare.

## Data availability

The data supporting this article have been included as part of the ESI.†

## Acknowledgements

This research was funded by the Russian Science Foundation (grant no. 21-72-10029), <https://www.rscf.ru/en/project/21-72-10029/> (accessed on 12 June 2025). The authors thank K. A. Bakina and R. N. Skandakov for their assistance in carrying out XAFS measurements.

## References

- C. Freire, M. Nunes, C. Pereira, D. M. Fernandes, A. F. Peixoto and M. Rocha, Metallo(salen) complexes as versatile building blocks for the fabrication of molecular materials and devices with tuned properties, *Coord. Chem. Rev.*, 2019, **394**, 104–134, DOI: [10.1016/j.ccr.2019.05.014](https://doi.org/10.1016/j.ccr.2019.05.014).
- R. M. Clarke and T. Storr, The chemistry and applications of multimetallic salen complexes, *Dalton Trans.*, 2014, **43**(25), 9380, DOI: [10.1039/c4dt00591k](https://doi.org/10.1039/c4dt00591k).
- A. K. Asatkar, M. Tripathi and D. Asatkar, *Salen and related ligands*, IntechOpen eBooks, 2020, DOI: [10.5772/intechopen.88593](https://doi.org/10.5772/intechopen.88593).
- M. Nunes, M. Araújo, J. Fonseca, C. Moura, R. Hillman and C. Freire, High-Performance Electrochromic Devices Based on Poly $[\text{Ni}(\text{salen})]$ -Type Polymer Films, *ACS Appl. Mater. Interfaces*, 2016, **8**(22), 14231–14243, DOI: [10.1021/acsami.6b01977](https://doi.org/10.1021/acsami.6b01977).
- O. V. Levin, M. P. Karushev, A. M. Timonov, E. V. Alekseeva, S. Zhang and V. V. Malev, Charge transfer processes on electrodes modified by polymer films of metal complexes with Schiff bases, *Electrochim. Acta*, 2013, **109**, 153–161, DOI: [10.1016/j.electacta.2013.07.070](https://doi.org/10.1016/j.electacta.2013.07.070).
- M. Vilas-Boas, C. Freire, B. De Castro, P. A. Christensen and A. R. Hillman, New Insights into the Structure and Properties of Electroactive Polymer Films Derived from  $[\text{Ni}(\text{salen})]$ , *Inorg. Chem.*, 1997, **36**(22), 4919–4929, DOI: [10.1021/ic970467j](https://doi.org/10.1021/ic970467j).
- S. V. Vasilieva, K. P. Balashev and A. M. Timonov, Effects of the nature of the ligand and solvent on the electrooxidation of complexes formed by Nickel and Schiff's bases, *Russ. J. Electrochem.*, 1998, **34**, 978–983.
- M. Vilas-Boas, I. C. Santos, M. J. Henderson, C. Freire, A. R. Hillman and E. Vieil, Electrochemical Behavior of a New Precursor for the Design of Poly $[\text{Ni}(\text{salen})]$ -Based Modified Electrodes, *Langmuir*, 2003, **19**(18), 7460–7468, DOI: [10.1021/la034525r](https://doi.org/10.1021/la034525r).
- A. A. Vereschagin, V. V. Sizov, P. S. Vlasov, E. V. Alekseeva, A. S. Konev and O. V. Levin, Water-stable  $[\text{Ni}(\text{salen})]$ -type electrode material based on phenylazosubstituted salicylic aldehyde imine ligand, *New J. Chem.*, 2017, **41**(22), 13918–13928, DOI: [10.1039/c7nj03526h](https://doi.org/10.1039/c7nj03526h).
- E. Dmitrieva, M. Rosenkranz, J. S. Danilova, E. A. Smirnova, M. P. Karushev, I. A. Chepurayana and A. M. Timonov, Radical formation in polymeric nickel complexes with N2O2 Schiff base ligands: An in situ ESR and UV–vis–NIR spectroelectrochemical study, *Electrochim. Acta*, 2018, **283**, 1742–1752, DOI: [10.1016/j.electacta.2018.07.131](https://doi.org/10.1016/j.electacta.2018.07.131).

- 11 A. Hamnett, J. Abel, J. Eameaim, P. Christensen, A. Timonov and S. Vasilyeva, A study of the polymerisation and electrochemical cycling of Pd methoxy-Salen derivatives using fast ellipsometry and FT-infrared spectroscopy, *Phys. Chem. Chem. Phys.*, 1999, **1**(22), 5147–5156, DOI: [10.1039/a906632b](https://doi.org/10.1039/a906632b).
- 12 M. Vilas-Boas, M. J. Henderson, C. Freire, A. R. Hillman and E. Vieil, A Combined Electrochemical Quartz-Crystal Microbalance Probe beam deflection (EQCM-PBD) study of solvent and ion transfers at a Poly[Ni(SaLTME)]-Modified electrode during redox switching, *Chem. - Eur. J.*, 2000, **6**, 1160–1167.
- 13 S. A. Krasikova, M. A. Besedina, M. P. Karushev, E. A. Dmitrieva and A. M. Timonov, In situ electrochemical microbalance studies of polymerization and redox processes in polymeric complexes of transition metals with Schiff bases, *Russ. J. Electrochem.*, 2010, **46**(2), 218–226, DOI: [10.1134/s102319351002014x](https://doi.org/10.1134/s102319351002014x).
- 14 E. A. Dmitrieva, S. A. Logvinov, V. V. Kurdakova, V. V. Kondrat'ev, V. V. Malev and A. M. Timonov, Redox polymer poly-N,N'-2,3-dimethylbutane-2,3-diyl-bis(salicylideneiminato) nickel: An impedance spectroscopy study, *Russ. J. Electrochem.*, 2005, **41**(4), 381–387, DOI: [10.1007/s11175-005-0079-y](https://doi.org/10.1007/s11175-005-0079-y).
- 15 M. Vilas-Boas, C. Freire, B. De Castro, P. A. Christensen and A. R. Hillman, Spectroelectrochemical characterisation of poly[Ni(saltMe)]-Modified electrodes, *Chem. - Eur. J.*, 2001, **7**, 139–150.
- 16 T. V. Semenistaya and G. A. Shagisultanova, Synthesis of new Cu(II), Ni(II), Pd(II), and Pt(II) complexes and conducting photosensitive polymers based on them, *Russ. J. Inorg. Chem.*, 2003, **48**, 520–527.
- 17 I. A. Chepurnaya, M. P. Karushev, E. V. Alekseeva, D. A. Lukyanov and O. V. Levin, Redox-conducting polymers based on metal-salen complexes for energy storage applications, *Pure Appl. Chem.*, 2020, **92**(8), 1239–1258, DOI: [10.1515/pac-2019-1218](https://doi.org/10.1515/pac-2019-1218).
- 18 C. E. Dahm, D. G. Peters and J. Simonet, Electrochemical and spectroscopic characterization of anodically formed nickel salen polymer films on glassy carbon, platinum, and optically transparent tin oxide electrodes in acetonitrile containing tetramethylammonium tetrafluoroborate, *J. Electroanal. Chem.*, 1996, **410**(2), 163–171, DOI: [10.1016/0022-0728\(95\)04520-1](https://doi.org/10.1016/0022-0728(95)04520-1).
- 19 J. Stöhr, *NEXAFS Spectroscopy*, 1992, DOI: [10.1007/978-3-662-02853-7](https://doi.org/10.1007/978-3-662-02853-7).
- 20 A. S. Vinogradov, S. I. Fedosenko, S. A. Krasnikov, A. B. Preobrajenski, V. N. Sivkov, D. V. Vyalikh, S. L. Molodtsov, V. K. Adamchuk, C. Laubschat and G. Kaindl, Low-lying unoccupied electronic states in 3d transition-metal fluorides probed by NEXAFS at the F1s threshold, *Phys. Rev. B:Condens. Matter Mater. Phys.*, 2005, **71**(4), 045127, DOI: [10.1103/physrevb.71.045127](https://doi.org/10.1103/physrevb.71.045127).
- 21 O. Bunău and Y. Joly, Self-consistent aspects of X-ray absorption calculations, *J. Phys.:Condens. Matter*, 2009, **21**(34), 345501, DOI: [10.1088/0953-8984/21/34/345501](https://doi.org/10.1088/0953-8984/21/34/345501).
- 22 A. L. Ankudinov, B. Ravel, J. J. Rehr and S. D. Conradson, Real-space multiple-scattering calculation and interpretation of X-ray-absorption near-edge structure, *Phys. Rev. B:Condens. Matter Mater. Phys.*, 1998, **58**(12), 7565–7576, DOI: [10.1103/physrevb.58.7565](https://doi.org/10.1103/physrevb.58.7565).
- 23 J. J. Rehr and R. C. Albers, Theoretical approaches to X-ray absorption fine structure, *Rev. Mod. Phys.*, 2000, **72**, 621–654, DOI: [10.1103/RevModPhys.72.621](https://doi.org/10.1103/RevModPhys.72.621).
- 24 P. M. Korusenko, O. V. Petrova and A. S. Vinogradov, Atomic and Electronic Structure of Metal-Salen Complexes [M(Salen)], Their Polymers and Composites Based on Them with Carbon Nanostructures: Review of X-ray Spectroscopy Studies, *Appl. Sci.*, 2024, **14**(3), 1178, DOI: [10.3390/app14031178](https://doi.org/10.3390/app14031178).
- 25 M. Newville, Fundamentals of XAFS, *Rev. Mineral. Geochem.*, 2014, **78**(1), 33–74, DOI: [10.2138/rmg.2014.78.2](https://doi.org/10.2138/rmg.2014.78.2).
- 26 G. J. Colpas, M. J. Maroney, C. Bagyinka, M. Kumar, W. S. Willis, S. L. Suib, P. K. Mascharak and N. Baidya, X-ray spectroscopic studies of nickel complexes, with application to the structure of nickel sites in hydrogenases, *Inorg. Chem.*, 1991, **30**(5), 920–928, DOI: [10.1021/ic00005a010](https://doi.org/10.1021/ic00005a010).
- 27 J. Tedim, A. Carneiro, R. Bessada, S. Patrício, A. L. Magalhães, C. Freire, S. J. Gurman and A. R. Hillman, Correlating structure and ion recognition properties of [Ni(salen)]-based polymer films, *J. Electroanal. Chem.*, 2007, **610**(1), 46–56, DOI: [10.1016/j.jelechem.2007.06.025](https://doi.org/10.1016/j.jelechem.2007.06.025).
- 28 T. Storr, E. C. Wasinger, R. C. Pratt and T. D. P. Stack, The Geometric and Electronic Structure of a One-Electron-Oxidized Nickel(II) Bis(salicylidene)diamine Complex, *Angew. Chem., Int. Ed.*, 2007, **46**(27), 5198–5201, DOI: [10.1002/anie.200701194](https://doi.org/10.1002/anie.200701194).
- 29 J. Tedim, R. Bessada, S. Patrício, A. L. Magalhães, C. Freire, S. J. Gurman and A. R. Hillman, Unusual Coordination Environment for Barium Cations in Ion Recognition Conducting Poly[Ni(salen)(receptor)] Films, *Langmuir*, 2008, **24**(16), 8998–9005, DOI: [10.1021/la801424k](https://doi.org/10.1021/la801424k).
- 30 J. Fonseca, J. Tedim, K. Biernacki, A. L. Magalhães, S. J. Gurman, C. Freire and A. R. Hillman, Structural and electrochemical characterisation of [Pd(salen)]-type conducting polymer films, *Electrochim. Acta*, 2010, **55**(26), 7726–7736, DOI: [10.1016/j.electacta.2010.01.073](https://doi.org/10.1016/j.electacta.2010.01.073).
- 31 M. Li, H. Jiao, H. Zhang and S. Jiao, Electrochemical polymerization of Schiff base transition metal polymer Poly[Ni(SALEN)] and its electrochemical performance in organic electrolyte, *Int. J. Electrochem. Sci.*, 2015, **10**(10), 8797–8806, DOI: [10.1016/s1452-3981\(23\)11137-0](https://doi.org/10.1016/s1452-3981(23)11137-0).
- 32 A. Gaur, B. D. Shrivastava, K. Srivastava, J. Prasad and S. K. Singh, XAFS investigations of copper(II) complexes with tetradentate Schiff base ligands, *X-Ray Spectrom.*, 2012, **41**(6), 384–392, DOI: [10.1002/xrs.2418](https://doi.org/10.1002/xrs.2418).
- 33 C. Johnson, B. Long, J. G. Nguyen, V. W. Day, A. S. Borovik, B. Subramaniam and J. Guzman, Correlation between Active Center Structure and Enhanced Dioxygen Binding in Co(salen) Nanoparticles: Characterization by In Situ Infrared, Raman, and X-ray Absorption Spectroscopies, *J. Phys. Chem. C*, 2008, **112**(32), 12272–12281, DOI: [10.1021/jp803985b](https://doi.org/10.1021/jp803985b).
- 34 V. S. Kshirsagar, A. C. Garade, R. B. Mane, K. R. Patil, A. Yamaguchi, M. Shirai and C. V. Rode, Characterization of clay intercalated cobalt-salen catalysts for the oxidation

- of p-cresol, *Appl. Catal., A*, 2009, **370**(1–2), 16–23, DOI: [10.1016/j.apcata.2009.09.003](https://doi.org/10.1016/j.apcata.2009.09.003).
- 35 J. Tedim, K. Biernacki, J. Fonseca, S. Patrício, A. Carneiro, A. L. Magalhães, S. J. Gurman, C. Freire and A. R. Hillman, Pseudo-crown functionalized copper salen complexes forming electroactive polymers: Rationalization of Ba<sup>2+</sup> interaction using XAS and DFT, *J. Electroanal. Chem.*, 2012, **688**, 308–319, DOI: [10.1016/j.jelechem.2012.09.036](https://doi.org/10.1016/j.jelechem.2012.09.036).
- 36 G. I. Svirskiy, A. V. Generalov, N. A. Vinogradov, X. O. Brykalova, A. V. Vereshchagin, O. V. Levin, A. G. Lyalin, A. B. Preobrajenski and A. S. Vinogradov, Electronic structure of the [Ni(Salen)] complex studied by core-level spectroscopies, *Phys. Chem. Chem. Phys.*, 2021, **23**(18), 11015–11027, DOI: [10.1039/d1cp00511a](https://doi.org/10.1039/d1cp00511a).
- 37 P. M. Korusenko, O. V. Petrova, A. A. Vereshchagin, K. P. Katin, O. V. Levin, S. V. Nekipelov, D. V. Sivkov, V. N. Sivkov and A. S. Vinogradov, A comparative XPS, UV PES, NEXAFS, and DFT study of the electronic structure of the Salen ligand in the H<sub>2</sub>(Salen) molecule and the [Ni(Salen)] complex, *Int. J. Mol. Sci.*, 2023, **24**(12), 9868, DOI: [10.3390/ijms24129868](https://doi.org/10.3390/ijms24129868).
- 38 P. M. Korusenko, A. V. Koroleva, A. A. Vereshchagin, D. V. Sivkov, O. V. Petrova, O. V. Levin and A. S. Vinogradov, The Valence band structure of the [Ni(SALen)] complex: an ultraviolet, soft x-ray and resonant photoemission spectroscopy study, *Int. J. Mol. Sci.*, 2022, **23**(11), 6207, DOI: [10.3390/ijms23116207](https://doi.org/10.3390/ijms23116207).
- 39 R. H. Holm; G. W. Everett and A. Chakravorty, Metal complexes of Schiff bases and B-Ketoamines, *Progress in Inorganic Chemistry*, 1966, pp. 83–214, DOI: [10.1002/9780470166086.ch3](https://doi.org/10.1002/9780470166086.ch3).
- 40 A. N. Yankin, D. A. Lukyanov, E. V. Beletskii, O. Y. Bakulina, P. S. Vlasov and O. V. Levin, Aryl-Aryl Coupling of Salicylic Aldehydes through Oxidative CH-activation in Nickel Salen Derivatives, *ChemistrySelect*, 2019, **4**(30), 8886–8890, DOI: [10.1002/slct.201902385](https://doi.org/10.1002/slct.201902385).
- 41 A. A. Chernyshov, A. A. Veligzhanin and Y. V. Zubavichus, Structural Materials Science end-station at the Kurchatov Synchrotron Radiation Source: Recent instrumentation upgrades and experimental results, *Nucl. Instrum. Methods Phys. Res., Sect. A*, 2009, **603**(1–2), 95–98, DOI: [10.1016/j.nima.2008.12.167](https://doi.org/10.1016/j.nima.2008.12.167).
- 42 W. E. O'Grady, K. I. Pandya, K. E. Swider and D. A. Corrigan, In situ X-Ray absorption Near-Edge structure evidence for quadrivalent nickel in nickel battery electrodes, *J. Electrochem. Soc.*, 1996, **143**(5), 1613–1617, DOI: [10.1149/1.1836687](https://doi.org/10.1149/1.1836687).
- 43 A. Espinosa, A. Serrano, A. Llavona, J. J. De La Morena, M. Abuin, A. Figuerola, T. Pellegrino, J. F. Fernández, M. Garcia-Hernandez, G. R. Castro and M. A. Garcia, On the discrimination between magnetite and maghemite by XANES measurements in fluorescence mode, *Meas. Sci. Technol.*, 2011, **23**(1), 015602, DOI: [10.1088/0957-0233/23/1/015602](https://doi.org/10.1088/0957-0233/23/1/015602).
- 44 A. M. Lebedev, K. A. Menshikov, V. G. Nazin, V. G. Stankevich, M. B. Tsetlin and R. G. Chumakov, NanoPES Photoelectron beamline of the Kurchatov Synchrotron radiation source, *J. Surf. Invest.: X-Ray, Synchrotron Neutron Tech.*, 2021, **15**(5), 1039–1044, DOI: [10.1134/S1027451021050335](https://doi.org/10.1134/S1027451021050335).
- 45 M. A. Siegler and M. Lutz, Ni(salen): a System That Forms Many Solvates with Interacting Ni Atoms, *Cryst. Growth Des.*, 2008, **9**(2), 1194–1200, DOI: [10.1021/cg801109n](https://doi.org/10.1021/cg801109n).
- 46 M. W. Schmidt, K. K. Baldrige, J. A. Boatz, S. T. Elbert, M. S. Gordon, J. H. Jensen, S. Koseki, N. Matsunaga, K. A. Nguyen, S. Su, T. L. Windus, M. Dupuis and J. A. Montgomery, General atomic and molecular electronic structure system, *J. Comput. Chem.*, 1993, **14**(11), 1347–1363, DOI: [10.1002/jcc.540141112](https://doi.org/10.1002/jcc.540141112).
- 47 A. D. Becke, Density-functional thermochemistry. III. The role of exact exchange, *J. Chem. Phys.*, 1993, **98**(7), 5648–5652, DOI: [10.1063/1.464913](https://doi.org/10.1063/1.464913).
- 48 C. Lee, W. Yang and R. G. Parr, Development of the Colle-Salvetti correlation-energy formula into a functional of the electron density, *Phys. Rev. B:Condens. Matter Mater. Phys.*, 1988, **37**(2), 785–789, DOI: [10.1103/physrevb.37.785](https://doi.org/10.1103/physrevb.37.785).
- 49 K. L. Schuchardt, B. T. Didier, T. Elsethagen, L. Sun, V. Gurumoorathi, J. Chase, J. Li and T. L. Windus, Basis Set Exchange: a community database for computational sciences, *J. Chem. Inf. Model.*, 2007, **47**(3), 1045–1052, DOI: [10.1021/ci600510j](https://doi.org/10.1021/ci600510j).
- 50 M. Newville, IFEFFIT: interactive XAFS analysis and FEFF fitting, *J. Synchrotron Radiat.*, 2001, **8**(2), 322–324, DOI: [10.1107/s0909049500016964](https://doi.org/10.1107/s0909049500016964).
- 51 S. A. Guda, A. A. Guda, M. A. Soldatov, K. A. Lomachenko, A. L. Bugaev, C. Lamberti, W. Gawelda, C. Bressler, G. Smolentsev, A. V. Soldatov and Y. Joly, Optimized finite difference Method for the Full-Potential XANES simulations: application to molecular adsorption geometries in MOFs and Metal-Ligand intersystem crossing transients, *J. Chem. Theory Comput.*, 2015, **11**(9), 4512–4521, DOI: [10.1021/acs.jctc.5b00327](https://doi.org/10.1021/acs.jctc.5b00327).
- 52 N. V. Tverdova, E. D. Pelevina, N. I. Giricheva, G. V. Girichev, N. P. Kuzmina and O. V. Kotova, Molecular structures of 3d metal complexes with various Schiff bases studied by gas-phase electron diffraction and quantum-chemical calculations, *J. Mol. Struct.*, 2011, **1012**, 151–161, DOI: [10.1016/j.molstruc.2011.06.037](https://doi.org/10.1016/j.molstruc.2011.06.037).
- 53 G. V. Girichev, N. I. Giricheva, N. P. Kuzmina, Y. S. Levina and A. Y. Rogachev, Molecular structure of NiO<sub>2</sub>N<sub>2</sub>C<sub>16</sub>H<sub>14</sub> from gas-phase electron diffraction and quantum chemical data, *J. Struct. Chem.*, 2005, **46**(5), 813–823, DOI: [10.1007/s10947-006-0205-z](https://doi.org/10.1007/s10947-006-0205-z).
- 54 V. V. Sizov, M. V. Novozhilova, E. V. Alekseeva, M. P. Karushev, A. M. Timonov, S. N. Eliseeva, A. A. Vanin, V. V. Malev and O. V. Levin, Redox transformations in electroactive polymer films derived from complexes of nickel with SalEn-type ligands: computational, EQCM, and spectro-electrochemical study, *J. Solid State Electrochem.*, 2014, **19**(2), 453–468, DOI: [10.1007/s10008-014-2619-4](https://doi.org/10.1007/s10008-014-2619-4).
- 55 D. A. Lukyanov, A. A. Vereshchagin, E. V. Beletskii, A. B. Atangulov, A. N. Yankin, V. V. Sizov and O. V. Levin, Nickel salicylidiminato 1D MOFS via electrochemical

- polymerization, *ChemElectroChem*, 2021, **9**(2), e202101316, DOI: [10.1002/celec.202101316](https://doi.org/10.1002/celec.202101316).
- 56 M. P. Feth, A. Klein and H. Bertagnolli, Investigation of the ligand exchange behavior of Square-Planar Nickel(II) complexes by X-ray absorption spectroscopy and X-ray diffraction, *Eur. J. Inorg. Chem.*, 2003, 839–852, DOI: [10.1002/ejic.200390114](https://doi.org/10.1002/ejic.200390114).
- 57 G. L. Miessler; P. J. Fischer and D. A. Tarr, *Inorganic chemistry*, Pearson, 5th edn, 2012.
- 58 A. F. Wells, *Structural inorganic chemistry*, Oxford University Press, USA, 2012.
- 59 T. Konishi, J. Kawai, M. Fujiwara, T. Kurisaki, H. Wakita and Y. Gohshi, Chemical shift and lineshape of high-resolution Ni K $\alpha$  x-ray fluorescence spectra, *X-Ray Spectrom.*, 1999, **28**(6), 470–477, DOI: [10.1002/\(sici\)1097-4539\(199911/12\)28:6](https://doi.org/10.1002/(sici)1097-4539(199911/12)28:6).
- 60 J. A. Bearden, X-Ray wavelengths, *Rev. Mod. Phys.*, 1967, **39**(1), 78–124, DOI: [10.1103/revmodphys.39.78](https://doi.org/10.1103/revmodphys.39.78).